

# Chapter 1

## Nuclear Radiation Detectors

### 1.1 Classification of Detectors

Experiments in Nuclear and Particle Physics depend upon the detection of primary radiation/particle and that of the product particles if any. The detection is made possible by the interaction of nuclear radiation with atomic electrons directly or indirectly. We may conveniently classify the detectors into two classes (i) Electrical (ii) Optical, as shown in Table 1.1.

The same detector may be used to study different types of radiation according to different phenomena. Thus, G.M. counters register all sorts of charged particles through ionization effects. Scintillation counters detect gamma rays by photoelectric effect, Compton scattering or pair production depending on gamma ray energy. Cerenkov counters detect a charged particle moving with speed exceeding that of light in a medium. Neutrons of high energy can be detected indirectly by the ionization caused by the recoil protons, and slow neutrons through the alpha particles produced in boron or by the fission of U-235 nuclei.

Instruments which provide one type of information accurately may give another type much less accurately. Thus, for example, semi-conductor detectors used to determine the energy of alpha particles yield precise determination of total energy released in an event but may furnish only a moderately accurate time resolution. Another example is the Cerenkov counter which furnishes accurate determination of the time at which an event occurs (within 1 nsec) but gives small spatial resolution. Photographic emulsions used to record the tracks of particles provide excellent spatial resolution but fail to distinguish between the old events and the new ones.

The detection efficiency of an instrument is of great consideration in an investigation. The detection efficiency which is the probability of detection when the particle crosses it, varies widely. In most of the direct ionizing radiation, it is nearly 1. In the detection of neutrons, it may vary from a few percent at high energy to nearly 1 for low energy. Similarly, gamma-ray counter efficiency is a function of energy.

**Table 1.1** Classification of detectors

Type	Detectors
Electric	Ionization Chamber
	Proportional Counter
	Geiger-Muller Counter
	Semi-conductor detector
	Neutron Detector
	Scintillation Counter
	Cerenkov Counter
Optical	Photographic Emulsion
	Expansion Cloud Chamber
	Diffusion Cloud Chamber
	Bubble Chamber
	Spark Chamber

The electric detectors necessarily carry auxiliary electronic equipment like pulse shapers, amplifiers, discriminators, coincidence circuits, scalars etc. Again, computers are invariably used to analyze more than hundred thousand pictures in a typical bubble chamber experiment.

After an event is detected, most of the instruments lose their sensitivity for certain time called “Dead time”. In order that the counter efficiency be high, it is important that the dead time be smaller than the mean time interval between successive events. If  $r$  is the counting rate and  $td$  is the dead time then for high efficiency, the condition  $rtd \ll 1$ , must be satisfied.

According to Hofstadter a perfect detector might have the following characteristics

- i. 100 percent detection efficiency
- ii. high-speed counting and timing ability
- iii. good energy resolution
- iv. linearity of response
- v. application to virtually to all types of particles and radiations
- vi. large dynamic range
- vii. virtually no limit to the highest energy detectable
- viii. reasonably large solid angles of acceptance
- ix. discrimination between types of particles
- x. directional information
- xi. low background, and
- xii. picturization of the event.

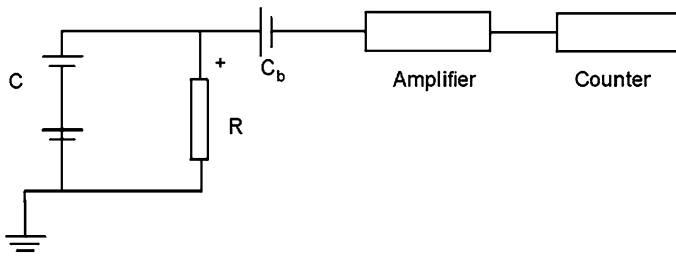


**Fig. 1.1** A pulse counting circuit

## 1.2 Ionization Chambers

### 1.2.1 Ionization Chambers

An ionization chamber is a device which measures the amount of ionization created by charged particles passing through a volume of gas enclosed in a vessel. If an electric field be maintained in a gas by a pair of electrodes, the positive and negative ions will drift apart inducing charges on the electrodes. In their traversal the ions may undergo recombination processes, and the charge collected by the electrodes alone will result in the ionization current measured in the external circuit. When every ion is collected, with no loss due to recombination, the maximum current is obtained called saturation current which will be proportional to the intensity of radiation.

### 1.2.2 Pulse Chambers

When an ionization chamber is exposed to a highly intense radiation the rate of ionizing events will be large. The ionization currents measured in the external circuit will be the average values, fluctuating about the mean value due to random fluctuations of events. For low intensity radiation it is often desirable to count primary individual events or pulses rather than register average values of current or voltage. In this case it is necessary to use short ion-collection and recovery time.

Applying Kirchhoff's law to the  $RC$  circuit (Fig. 1.1) it is found that the signal voltage developed across  $R$  is given by

$$V = \left( \frac{Q}{C} \right) e^{-\frac{t}{RC}} \quad (1.1)$$

where  $C$  is the capacitance of the chamber. Equation (1.1) shows that the polarity of the pulse will be opposite to that of the applied voltage. The peak amplitude of the signal is determined by the ratio  $Q/C$  and the rate of decay by the product  $RC$ .

The product  $RC$  is called the time constant. At time  $t = RC$ , the pulse amplitude will be reduced to  $1/e = 0.37$  of its peak value. If  $R$  is in ohms and  $C$  in farads

then  $t$  is in seconds. For pulse counting, it is desirable to choose the time constant  $10^{-4}$  or less. In Fig. 1.1,  $C_b$  is the blocking capacitor to isolate the recording circuits from D.C. high voltage. The output in the form of a pulse is passed on to the A.C. amplifier and a counter.

### 1.2.3 Gas-Filled Pulse Counter

Most of the gas-filled pulse counters take the advantage of large multiplication of ion pairs, through the occurrence of secondary ionization. This is called gas multiplication. The ions are accelerated towards the charged electrodes until re-combination takes place or lose their energy through a collision. At atmospheric pressure, under moderate electric fields, the mean free path between successive collisions is short and the energy acquired by an ion between collisions is small and the collisions are mainly elastic. However, if the gas pressure is reduced or if the applied voltage is substantially increased, an ion can pick up appreciable energy and the occurrence of inelastic collisions becomes a distinct possibility. The inelastic collisions result in the molecular excitation or ionization. An additional ion pair is caused by ionization. The secondary ions produce tertiary ions and so on in the subsequent collisions, thus producing enormously large number of ion pairs. This kind of multiplication process is called avalanche ionization. If a single primary pair finally results in  $A$  ion pairs then the gas multiplication is  $A$ . In an ionization chamber  $A$  will be unity as no secondaries are formed and may be as large as  $10^{10}$  in a Geiger-Muller tube.

#### 1.2.3.1 Geometry of the Chamber

For the plane parallel electrodes field strength  $E$  is given by

$$E = \frac{V}{d} \quad (1.2)$$

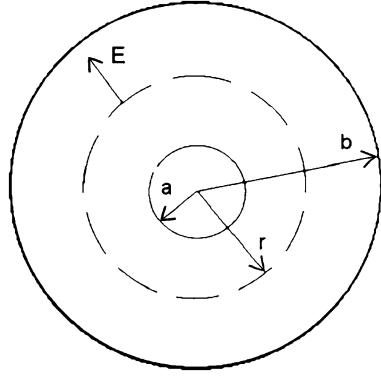
Now, for gas amplification in a mean free path an ion must pick up enough energy to ionize a neutral molecule. For typical ionization potentials which range from 10–25 eV, the field strength required is of the order of  $10^6$  volts  $\text{cm}^{-1}$ . Such field strengths are not practical.

The mean-free-path can be increased by reducing the pressure is determined by making a compromise between these conflicting requirements. Even with the best choice of gas pressure, the electric field requirement is much excessive for plane geometry. However, other type of geometry for the electrodes, in particular that of a co-axial cylinder, permits the use of gas at moderate pressure, a large field strength without employing very high voltages.

Consider an outer cylinder as the cathode with a coaxial wire of smaller diameter as the anode. Figure 1.2 shows the cross-section of the cylindrical configuration.

The cathode has radius  $b$  and the anode radius  $a$ . Consider a cylindrical surface of radius  $r$  in between.

**Fig. 1.2** Cross section of a counter with cylindrical geometry



The normal component of electric field acts radially outward and is constant. Applying Gauss theorem to the surface,

$$\oint E_n ds = 2\pi r E = \frac{q}{\epsilon} \quad (1.3)$$

where  $E_n = E = \text{constant}$ . Integration is done only on the cylindrical surface since the normal component at the closed surfaces is zero.

The potential difference between the two electrodes is given by

$$V = \int_a^b E_n dr = \frac{q}{2\pi\epsilon} \int_a^b \frac{dr}{r} = \frac{q}{2\pi\epsilon} \ln \frac{b}{a} \quad (1.4)$$

Combining (1.3) and (1.4),

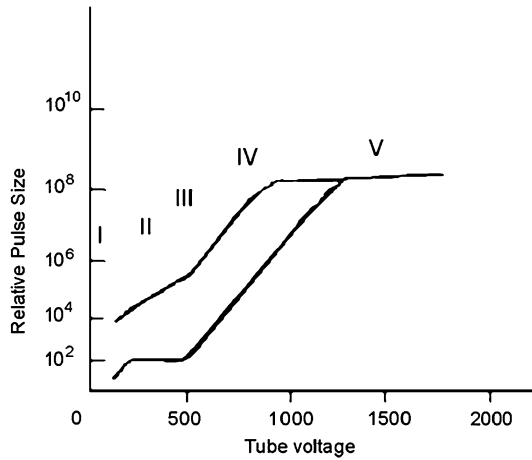
$$E = \frac{V}{r \ln(\frac{b}{a})} \quad (1.5)$$

For given values of  $a$  and  $b$ , the most intense field will be close to the surface of the wire. Equation (1.5) shows that for a given voltage large values of  $E$  can be obtained for small diameter anode wire. Structural strength requirements limit the minimum diameter to 0.08 mm.

### 1.2.4 Variation of Pulse Sizes

We now consider the pulse sizes produced by a radiation source of constant intensity. At low voltages, the counter behaves as an ionization chamber (Region I, Fig. 1.3). This is a recombination region. As the applied voltage is increased, saturation region II is reached. The larger size pulse has been taken as  $10^3$  times greater than the smaller size pulse for illustration. With further increase of voltage secondary ioniza-

**Fig. 1.3** Comparative pulse sizes from a small and large size primary ionizing event with gas amplification



tion ensues. Secondary ions will be produced when the integral of (1.4) taken over one mean-free-path equals the ionization potential of the counter gas. Secondary ionization will occur over the mean-free-path that lies just outside the central wire since the electric field is maximum close to the central wire. Primary ions formed outside of this mean-free-path experience a weaker field. They will be accelerated towards the respective electrodes but will not acquire enough energy to generate secondaries.

With the initiation of secondary ionization, each pulse will be enhanced compared to that of the primary ions alone by a factor which depends on the voltage but not upon the number of primary ions. The size of each pulse is proportional to the size of the primary initiating ionization by a constant factor. This is the proportional region III, Fig. 1.3. With further increase of voltage, secondary ionization may be produced beyond one mean-free-path from the central wire. The gas amplification will increase but the proportionality factor will be maintained until a gas amplification factor of about  $10^4$  is reached.

As the voltage is further increased, secondary ions will be formed farther and farther from the wire until gas amplifications of  $10^5$ – $10^7$  are reached. This is the region of limited proportionality (Region IV). Here the proportionality becomes weaker and weaker until it is lost. The two curves merge into one.

With further increase of voltage larger avalanche results until in the Geiger region (region V), as many as  $10^{10}$  secondary ion pairs may be produced from a single ion pair. Here the size of the output pulse is saturated. In this region each pulse of ionization spreads axially along the entire length of the wire and radially it extends outward over several mean-free-paths.

Beyond Geiger's plateau there is a voltage breakdown and continuous discharge takes place.

## 1.3 Proportional Counter

### 1.3.1 Construction

Gas proportional counters usually have spherical or semi-hemispherical geometry. They are used when extreme values of gas amplification  $A$  are not required. A typical value of  $A$  may be  $10^3$ . In the hemispherical type the anode is in the form of a small loop. The electric field changes rapidly in the vicinity of the anode as in the case of a cylindrical counter. The voltage-pulse size relations are also similar.

In the proportional region, with a typical gas amplification of  $10^3$ , the pulse generated by alpha might contain  $10^8$  ions while for beta particles or gamma rays the corresponding figure is about  $10^5$ . Even with these amplifications the pulses are not large enough to be detected. A pre-amplifier, with little gain serves the purpose of producing an output signal across a relatively low impedance. This is followed by a linear amplifier with voltage gain 200–500 and is used to amplify the pulse preserving the relative size. A discriminator allows only those pulses which are above a certain level. In this manner, all the small pulses due to beta particles and gamma rays are rejected and only relatively larger pulses due to alpha particles are counted. Similarly fission pulses can be counted against heavy background of alpha particles. Figure 1.4 is a representative diagram of a spherical chamber with  $4\pi$  geometry. Window absorption can be introduced directly into the sensitive volume of the chamber. The source is placed on a thin film to minimize back scattering and self absorption. Filling gas at suitable pressure is flushed into the chamber to displace the air. Such a chamber is called windowless gas-flow counter. For the filling gas, pure Argon, though highly dense, is not suitable as the meta-stable states which are formed upon de-excitation after a relatively long time lead to spurious discharges. However, 90 percent argon and 10 percent methane mixture or a 96 percent Helium and 4 percent isobutane are commonly used. A voltage of 1500–4000 volts is generally used.

The advantage of the  $4\pi$  windowless counter, Fig. 1.4, is that all the particles are counted and is therefore ideal for the absolute decay rate determinations of radioactive substances. Proportional counters are very useful for high counting rates, because the negative ions have to move only a few mean-free-paths to be collected in an intense electric field.

## 1.4 Geiger Muller Counter

### 1.4.1 Construction and Characteristics

Geiger Muller Counter (GM counter) is one of the old devices used to detect charged particles, regardless of their energy and identity. Nevertheless, it is by no means outdated. Figure 1.5 shows the GM tube along with the block diagram of the electronic circuit.

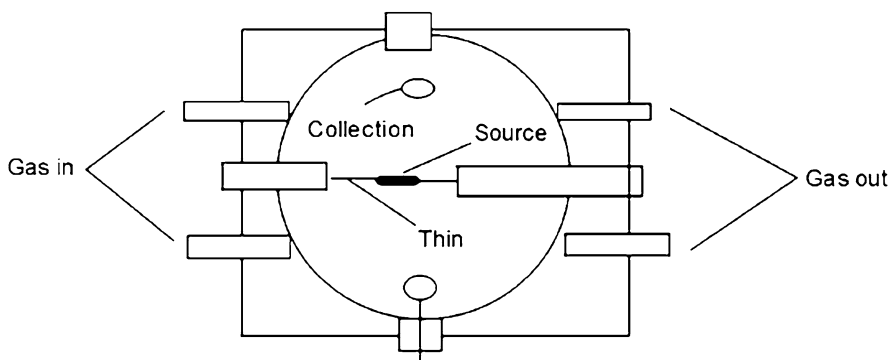


Fig. 1.4 Representative diagram of a spherical chamber with  $4\pi$  geometry

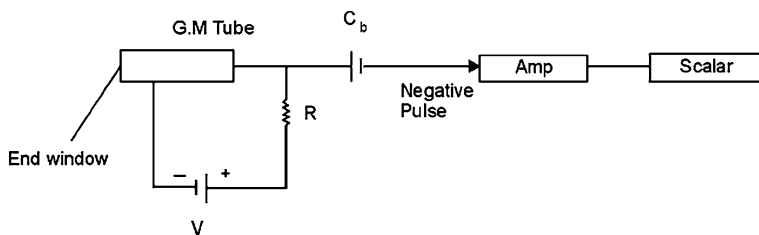


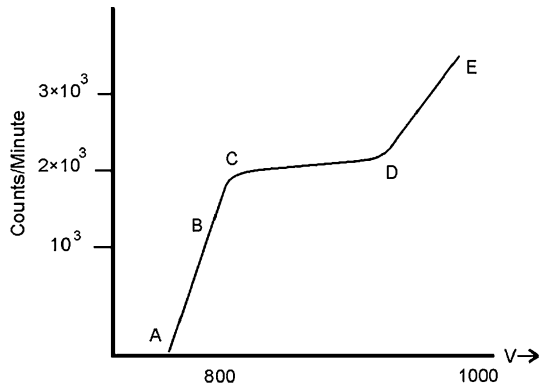
Fig. 1.5 A GM tube circuit when GM tube is operated, a negative pulse is developed for the output

The GM tube is usually of a cylindrical geometry, the outer hollow cylinder of diameter 1–10 cm and length 2–10 times as great, forms the cathode and the inner central wire of small radius, concentric with outer cylinder forms the anode. Cathode surface is coated with a substance to provide a large work function. The central wire is usually made of tungsten, tantalum or stainless steel with a smooth surface and of desired diameter. End-windows as thin as  $1 \text{ mg cm}^{-2}$  made of cleaved mica or thin glass permit low energy beta particles to be counted. A high voltage of 800 V to 1100 V is generally used. The blocking capacitor  $C_b$  (Fig. 1.5) isolates the electronic circuit from the high voltage that is applied but permits the pulses developed across the resistor  $R$  to get through, and recorded by the electronic circuit.

Let a GM tube in such a circuit be exposed to radiation of constant intensity. There is a threshold A as the circuits do not respond below it, Fig. 1.6. The threshold generally corresponds to the region of limited proportionality, where the gas amplification is of the order of  $10^6$ – $10^7$ . With the increase of voltage above threshold, the count rate rises sharply through B, as the small primary events also get counted. The point C is the beginning of the Geiger region and extends up to D, the flat part of the curve CD is called plateau. In the region CD where every event regardless of its original size is counted. Actually a plateau has a small upward slope. GM tubes with plateau length 200 volts and a change of counting rate of only 1–2 percent for a change 100 volts are available. The length as well as slope of plateau depend



**Fig. 1.6** Typical variation of counting rate as a function of applied voltage for a GM tube



on several factors, such as the filling gas, the condition of central wire and cathode surface.

When the voltage is further raised, beyond the end of plateau, multiple discharge called continuous discharge occurs, in the region E. Continuous discharge may be triggered by a single pulse. The continuous discharge rate will be independent of any radiation-initiated event and will depend only on the circuit elements. GM tubes are not operated in this region. If operated, the life would be shortened or the tube may even be damaged beyond repair.

### 1.4.2 Pulse Formation and Decay

The initial ionization pulse which consists of equal number of positive ions and electrons is formed as a thin cylindrical sheath just outside the central wire. Immediately, the ions start separating, the electrons moving toward the central wire and the positive ions outward toward the cathode. Because of their high mobility, the electrons are collected at the wire in a short time of the order  $10^{-5}$  sec, while the positive ion cloud (space charge) will be still close to the wire.

Let the space charge move outward to a distance  $r_0$ , Fig. 1.7, after some time. Let there be  $q^-$  charges per unit length on the wire and  $q^+$  charges per unit length in the space charge. The field intensity  $E_1$  inside the sheath will be different from  $E_2$  outside.

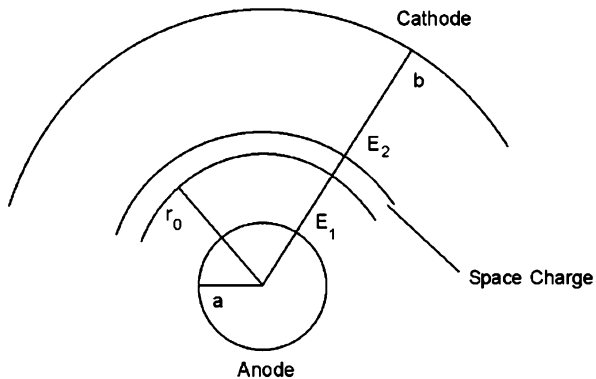
From (1.3),

$$E_1 = \frac{q^-}{2\pi\epsilon r} \quad (\text{inside}) \quad (1.6)$$

$$E_2 = \frac{q^- + q^+}{2\pi\epsilon r} \quad (\text{outside}) \quad (1.7)$$

Assuming that the applied voltage is constant, the voltage developed is given by the integrals of the field strengths.

**Fig. 1.7** The positive ion space charge moves toward the cathode



$$\begin{aligned}
 V &= \int_a^{r_0} \frac{q^- dr}{2\pi \epsilon r} + \int_{r_0}^b \frac{(q^- + q^+) dr}{2\pi \epsilon r} \\
 &= \frac{q^-}{2\pi \epsilon} \ln \frac{r_0}{a} + \frac{(q^- + q^+)}{2\pi \epsilon} \ln \frac{b}{r_0} \\
 &= \frac{q^-}{2\pi \epsilon} \ln \frac{b}{a} + \frac{q^+}{2\pi \epsilon} \ln \frac{b}{r_0}
 \end{aligned}$$

The charge on the central wire will be

$$q^- = \frac{2\pi \epsilon}{\ln(b/a)} \left[ V - \frac{q^+}{2\pi \epsilon} \ln \frac{b}{r_0} \right] \quad (1.8)$$

Equation (1.8) shows that both  $q^-$  and  $E_1$  in the avalanche region are reduced during the pulse. As the positive ion sheath moves toward the cathode,  $r_0$  increases, the negative term in (1.8) decreases and the field strength is restored to its original value in the state prior to ionization.

A typical time in which the positive-ion cloud reaches the cathode is of the order of  $10^{-4}$  sec. When a positive ion comes within about  $10^{-7}$  cm from the cathode, it will capture an electron from the cathode surface to become a neutral molecule. In this process the molecule will get into an excitation state. As a result of de-excitation, photons will be emitted, some of them in the ultra violet region. These photons upon hitting nearby cathode surface will liberate electrons by photoelectric effect. The photo electrons thus liberated will now be accelerated toward the anode. Upon reaching the vicinity of the wire, they would have acquired sufficient energy to initiate a secondary avalanche. Thus a single discharge will eventually lead to a series of discharges at a rate determined by the parameters of the counter and the circuit.

### 1.4.3 Quenching the Discharge

From the discussion at the end of Sect. 1.4.2, it is obvious that there must be a mechanism for stopping the occurrence of repetitive discharges. This mechanism is called

Quenching. In practice this is accomplished by making the counter self- quenching on adding a small percentage of a quenching gas to the main gas. The main gas is usually argon and the quenching gas can be either organic such as alcohol, xylene or isobutane or halogen gases like  $\text{Cl}_2$  or  $\text{Br}_2$ .

Consider a GM counter filled with a mixture of 90 % argon and 10 % of ethyl alcohol at 10 cm of mercury. In the first phase of avalanche the space-charge will contain both types of positive ions. Now the ionization energy of argon atom is 15.7 eV while for ethyl alcohol molecule, it is 11.3 eV. In an argon-alcohol collision, it is energetically possible for the argon to become neutral, while alcohol molecule is ionized. On the other hand, it is not energetically possible for an alcohol molecule to become neutral while argon atom is ionized. Each ion will make some thousand collisions while the space charge is on its way to the cathode. Before the space charge reaches the cathode, it now almost entirely consists of alcohol ions.

On reaching close to the cathode surface, the alcohol ion picks up an electron and the excitation energy is given by

$$E^* = I - \varphi \quad (1.9)$$

where  $I$  is the ionization potential of alcohol and  $\varphi$  is the work function of the cathode material. If a cathode surface of large work function be chosen, such as colloidal ( $\varphi = 5$  eV) then less excitation energy will be available for the alcohol molecule. The de-excitation via molecular dissociation is strongly favored compared to radiation. The photon energies involved in the dissociation process are too small to initiate a second discharge. In the event of de-excitation by radiation, most of the resulting photons will have energy much below the work function of the cathode, and the photo electron emission would be energetically impossible. In each collision the energy transfer from argon to alcohol results in the emission of photons of energy  $15.7 - 11.3 = 4.4$  eV, a value much below the work function of the selected cathode surface. Most of the photons emitted will be reabsorbed in the broad bands in the ultraviolet. Occasionally, an argon ion may escape and may extract an electron from the cathode. By (1.9) the excitation energy will be in excess of 4.4 eV compared to that in alcohol. This increases the probability for photon emission and hence photo-electric emission from the cathode surface. As the voltage increases the transit time decreases and further the ion density in the original plasma will be greater. This leads to occasional spurious discharges. The upward slope of the plateau is attributed to this phenomenon. With further increase in voltage, the occurrence of spurious discharges becomes a dominant phenomenon (Fig. 1.8). One must avoid working the GM tube in this region otherwise, the life of the tube may be shortened or it may be irreparably damaged.

When organic quenching gases are used some of the molecules are dissociated in each discharge. In a typical counter there may be  $10^{20}$  molecules of alcohol. In each pulse  $10^{10}$  molecules may be dissociated. Theoretically,  $10^{10}$  pulses can be counted. But much before theoretical limit is reached, the counter starts behaving erratically. The life of such counters is therefore finite.

When halogens like  $\text{Cl}_2$  are used as a quenching gas, the dissociated molecules of  $\text{Cl}_2$  by recombination process become neutral again, and are therefore available

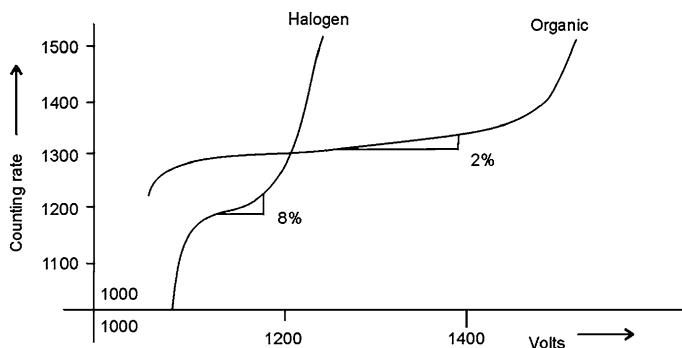


**Fig. 1.8** Typical plateau slopes for halogen and organic quenched GM counters

for subsequent discharges. Theoretically, such counters have infinite life time. The plateau, however, is inferior than that for organic counters. Typical plateau length is limited to 150 V, with a slope of 8 % per 100 V length. These values are to be compared with 300 V length and 2 % slope for organic counters, Fig. 1.8.

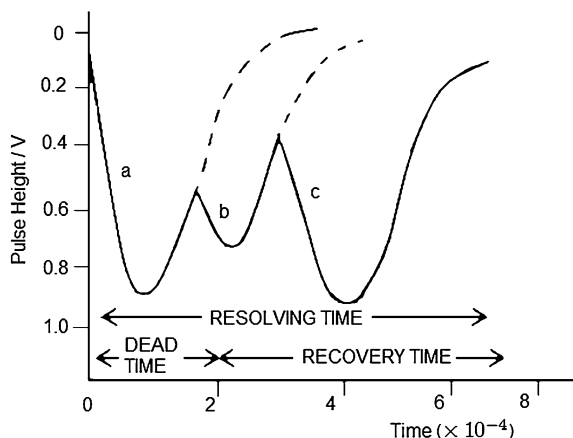
### 1.4.4 Scaling Circuits

The pulses from a GM counter are negative, rising to maximum amplitude of about 1 volt in a time of the order of  $10^{-5}$  sec and decaying in about  $10^{-3}$  sec. It is preferable to amplify the pulses before feeding them to a counting system. As the mechanical register cannot respond to fast occurring pulses they are passed through a scalar. A binary scalar consists of several bi-stable circuits in tandem. At each stage a single pulse is transmitted for every two pulses received. At each stage the counts are cut down by a factor 2. Thus, the scaling factors of 2, 4, 8, 16, 32, 64, ... will be available. A binary scalar can be converted into a decade scalar. With the use of a suitable feedback circuit, a scale of 16 can be reset to zero at the tenth pulse. A timer is automatically actuated at the moment the push-button is on, and the counting is stopped after a fixed duration. The counting rate is then simply found out.

## 1.5 Resolving Time

It has been pointed out that the space charge reduces the gas amplification to the extent that the secondary ionization temporarily becomes impossible. During this interval of time no event can be recorded. This is called **Dead Time**. As the space charge moves out toward cathode, its effect on the electric field in the immediate neighborhood of the central wire gradually decreases until the original voltage is

**Fig. 1.9** Dead time, Recovery time and Resolving time of a GM tube and counting circuit



restored. Suppose a pulse of minimum amplitude of 0.5 volts is required to get it registered. Consider three pulses *a*, *b*, and *c*, Fig. 1.9, caused by three particles.

Pulse *a* starts at time  $t = 0$  and has full amplitude of 0.9 V at  $1.0 \times 10^{-4}$  sec, and will certainly be counted. Due to arrival of a second particle, pulse *b* starts at time  $1.8 \times 10^{-4}$  sec and builds up to 0.1 V at maximum amplitude and will not be counted. At  $t = 3.0 \times 10^{-4}$  sec, the pulse *c* starts due to the third particle, but has maximum amplitude of 0.5 V at  $t = 4.0 \times 10^{-4}$  sec, barely sufficient to actuate the counting system. The time  $\tau$  between just recordable pulses is known as the **Resolving Time**. It is obvious that because of finite resolution time, some of the random pulses will be lost.

$$\text{Resolving time} = \text{Dead time} + \text{Recovery time}$$

Let the true counting rate be  $N$ , i.e. without losses due to finite resolution, and  $n$  observed counting rate. The insensitive time will be  $n\tau$  per unit time and the number of counts missed will be  $Nn\tau$  which is also equal to  $N - n$ . Hence

$$N - n = Nn\tau \quad \text{or} \quad N = \frac{n}{1 - n\tau} \quad (1.10)$$

### 1.5.1 Determination of Resolving Time: Double Source Method

This method involves four counts using two radioactive sources. First, the background rate  $B$  per sec is found. One of the sources is then positioned in such a way that the resolving time losses are substantial. Let the expected count rate be  $N_1 + B$  and that observed  $n_1 + B$ . With the first source still in position the second one is introduced and adjusted until the count rate is approximately doubled.

Then the expected count rate is  $N_1 + N_2 + B$  and the observed count rate is  $n_{12} + B$ .

Finally the first source is removed and the second is left in position.

Then the expected count rate is  $N_2 + B$  and the observed count rate is  $n_2 + B$ .

$$N_1 + N_2 = N_{12} + B \quad (1.11)$$

$$\frac{n_1}{1 - n_1\tau} + \frac{n_2}{1 - n_2\tau} = \frac{n_{12}}{1 - n_{12}\tau} + \frac{B}{1 - B\tau} \quad (1.12)$$

$n_1$  and  $n_2$  will be of the order of 100 per sec,  $n_{12}$  of the order of 200 per sec,  $B \cong 1$  per sec and  $\tau \cong 10^{-4}$  sec, so that  $n_1\tau \ll 1$ ,  $n_2\tau \ll 1$ ,  $n_{12}\tau \ll 1$ ,  $B\tau \ll 1$ , and (1.12) can be approximated to

$$\begin{aligned} n_1(1 + n_1\tau) + n_2(1 + n_2\tau) &= n_{12}(1 + n_{12}\tau) + B \\ n_1 + n_2 - n_{12} - B &= \tau[n_{12}^2 - n_1^2 - n_2^2] \cong \tau[(n_1 + n_2)^2 - n_1^2 - n_2^2] \quad \text{or} \\ \tau &= \frac{n_1 + n_2 - n_{12} - B}{2n_1n_2} \end{aligned} \quad (1.13)$$

## 1.6 Resolving Time of a Coincidence Circuit

As the pulses arriving at the input of the coincidence circuit will have finite width, two independent (not coincident) signals may give rise to a pulse in the output (spurious coincidence or chance coincidence or accidental coincidence) if their relative delay is smaller than a certain time  $\tau$ , the resolving time. Their number per unit time  $C_c$  depends on the single counting rates  $m_1$  and  $m_2$  of the two counters. The probability that a certain pulse from the first counter is accompanied by a pulse from the second counter within  $\pm\tau$  is  $p \cong m_1m_2(2\tau)$ . The number of chance coincidences is therefore

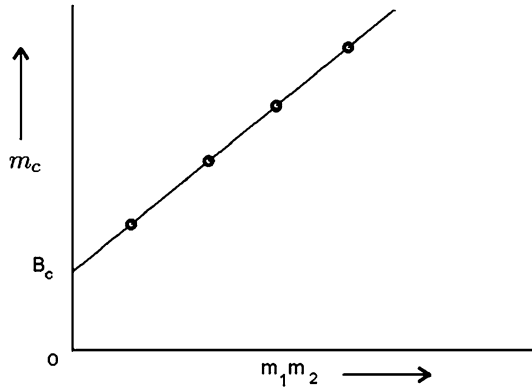
$$C_c = 2\tau m_1m_2 \quad (1.14)$$

### 1.6.1 Determination of the Resolving Time of the Coincidence Circuit

Two independent sources are used and counting is made with two counters. They are well shielded from each other so that no genuine coincidence is registered. The observed coincidences are then only due to the finite resolving time and to the background produced by cosmic rays. Cosmic rays flux is maximum from the top, and if the counters are placed above each other, a single cosmic ray particle can penetrate both and produce a coincidence. On the other hand if they are placed horizontally, they can be triggered only by at least two shower particles which come from the same source. These are rather rare events. Thus the cosmic background  $B_c$  produced by the cosmic rays depends strongly on the relative position of the counters. If coincidence counting rate  $m_c$  is measured for different counting rate for different source strengths, the coincidence rate is given by

$$m_c = B_c + 2\tau m_1m_2 \quad (1.15)$$

**Fig. 1.10** Determination of resolving time. Plot of  $m_c$  against  $m_1 m_2$



Assuming that  $\tau$  is constant, the plot of  $m_c$  vs.  $m_1 m_2$  is a straight line intercepting at the background value  $B_c$  and having a slope equal to  $2\tau$ , Fig. 1.10.

### 1.6.1.1 Limitation of the Useful Source Strength by the Resolving Time

It is desirable that the number of chance coincidences be smaller than the number of true coincidences. As an example, consider the beta emission from a certain isotope followed by gamma emission. If  $D$  is the source strength, beta and gamma counting rates are

$$m_\beta = D P_\beta \quad (1.16)$$

$$m_\gamma = D P_\gamma \quad (1.17)$$

where  $P_\beta$  and  $P_\gamma$  are the probabilities of detecting a given beta particle in the beta counter and the gamma counter, respectively. The probability of detecting a beta ray and at the same time in coincidence a gamma ray is the product of the two probabilities. The true coincidence is then

$$m_{\beta\gamma} = D P_\beta P_\gamma \quad (1.18)$$

On the other hand, the chance coincidence is

$$C_c = 2\tau m_\beta m_\gamma = 2\tau D^2 P_\beta P_\gamma \quad (1.19)$$

The condition  $C_c < m_{\beta\gamma}$  becomes

$$2\tau D < 1 \quad (1.20)$$

For the resolving time of 1  $\mu\text{sec}$ , the source strength must be smaller than  $5 \times 10^5$  decays/sec i.e. smaller than 13.5  $\mu\text{ci}$ .

**Example 1.1** An ionization chamber is used with an electrometer capable of measuring  $5 \times 10^{-11}$  ampere to assay a source of 0.7 MeV beta particles. Assuming saturation conditions and that all the particles are stopped within the chamber, calculate the rate at which the beta particles must enter the chamber to just produce a measurable response. Given the ionization potential for the gas atoms is 35 eV.

**Solution** Let  $N$  beta particles enter the chamber per second. Number of ion pairs released,

$$n = \frac{0.7 \times 10^6}{35} = 2 \times 10^4$$

The current will be  $Nne = i$

$$N = \frac{i}{ne} = \frac{5 \times 10^{-11}}{2 \times 10^4 \times 1.6 \times 10^{-19}} = 1.56 \times 10^4 \text{ beta particles/sec}$$

**Example 1.2** Estimate the gas multiplication required to count a 1 MeV proton which gives up all its energy to the chamber gas in a proportional counter. Assume that the amplifier input capacitance in parallel with the counter is  $1 \times 10^{-9}$  F and that its input sensitivity is 1 mV. Energy required to produce one ion pair is 35 eV.

**Solution**

$$V = \frac{MNq}{C}$$

$$M = \frac{CV}{qN} = \frac{10^{-9} \times 10^{-3}}{1.6 \times 10^{-19} \times (10^6/35)} = 219$$

**Example 1.3** A proportional counter is used with an electrometer capable of measuring  $5 \times 10^{-11}$  Ampere to assay a source of 0.7 MeV beta particles. The beta particles produce on an average 60 ion pairs with a gas multiplication factor of  $6 \times 10^4$ . What rate of particle incidence will be required to produce an average current of  $5 \times 10^{-11}$  ampere?

**Solution** Let  $N$  beta particles be incident per second.

Current  $i = NnMe$ , where  $n$  is the number of ion pairs

$$N = \frac{i}{nMe} = \frac{5 \times 10^{-11}}{60 \times 6 \times 10^4 \times 1.6 \times 10^{-19}} = 87$$

**Example 1.4** Calculate the pulse height obtained from a proportional counter when a 10 keV electron gives up all its energy to the gas. The gas multiplication factor of the proportional counter is 800, capacitance of the circuit is  $20 \times 10^{-12}$  F and energy required to produce an ion pair is 32 eV.

**Solution** Number of primary ion pairs produced by a 10 keV electron,

$$N = 10^4/32$$

$$\text{Charge collected } Q = Mne$$

where  $M$  is the gas multiplication and  $e$  the elementary charge is equal to  $1.6 \times 10^{-19}$  Coulomb.

Pulse height obtained is



$$V = \frac{Q}{C} = \frac{MNe}{C} = \frac{800}{20 \times 10^{-12}} \times \left( \frac{10^4}{32} \right) \times 1.6 \times 10^{-19}$$

$$V = 2 \times 10^{-3} \text{ volt}$$

$$= 2 \text{ mV}$$

**Example 1.5** Calculate the resolving time of a GM counter from the following observations by the double source method: Background count 60 cpm, first source in position 8220 cpm, both sources in position 16,860 cpm, second source in position 9360 cpm.

### Solution

$$B = 60 \text{ cpm} = 1 \text{ cps}$$

$$n_1 + B = 8220 \text{ cpm} = 137 \text{ cps}$$

$$n_{12} + B = 16,860 \text{ cpm} = 281 \text{ cps}$$

$$n_2 + B = 9,360 \text{ cpm} = 156 \text{ cps}$$

$$\tau = \frac{n_1 + n_2 - n_{12} - B}{2n_1n_2}$$

$$= \frac{(137 - 1) + (156 - 1) - (281 - 1) - 1}{2(137 - 1)(156 - 1)}$$

$$= 240.8 \times 10^{-6} \text{ sec}$$

$$= 241 \text{ } \mu\text{sec}$$

**Example 1.6** A counting rate of 16,200 counts/min is indicated by a GM tube having a dead time of 250  $\mu\text{sec}$ . Calculate the counting rate that would be observed in the absence of dead time loss.

### Solution

$$N = \frac{n}{1 - n\tau} = \frac{16200}{1 - \frac{16200}{60} \times 250 \times 10^{-6}} = 17,373 \text{ counts/min}$$

**Example 1.7** The plateau of a G.M. counter working at 1 kV has a slope of 2.5 % count rate per 100 V. By how much can the working voltage be allowed to vary if the count rate is to be limited to 0.1 %?

### Solution

$$\text{Slope} = \frac{n_2 - n_1}{n_{av}} \times \frac{100}{V_2 - V_1} \times 100 \text{ percent per } 100 \text{ V}$$

$$\text{Given } \frac{n_2 - n_1}{n_{av}} = \frac{0.1}{100}$$

$$\text{Slope} = \frac{0.1}{100} \times \frac{100}{\Delta V} \times 100 = 2.5$$

or

$$\Delta V = \frac{10}{2.5} = 4 \text{ volts}$$

The voltage should not vary more than  $\pm 2$  volts from the operating voltage of 1 kV.

*Example 1.8* An organic-quenched G.M. tube has the following characteristics.

Working voltage 1000 V  
 Diameter of anode 0.2 mm  
 Diameter of cathode 2.0 cm  
 Maximum life time  $10^9$  counts

What is the maximum radial field in the tube and how long will it last if used for 15 hr per week of 6000 counts per minute?

**Solution**

$$E = \frac{V}{r \ln(b/a)}$$

Field will be maximum close to the anode.

$$r = 0.1 \text{ mm} = 1 \times 10^{-4} \text{ m}$$

$$E_{\max} = \frac{1000}{10^{-4} \times \ln(20/0.2)} = 2.17 \times 10^6 \text{ V/m}$$

The lifetime of G.M. tube in years is given by dividing total number of counts possible by counts per year.

$$t = \frac{10^9}{52 \times 15 \times 6000 \times 60} = 3.56 \text{ years.}$$

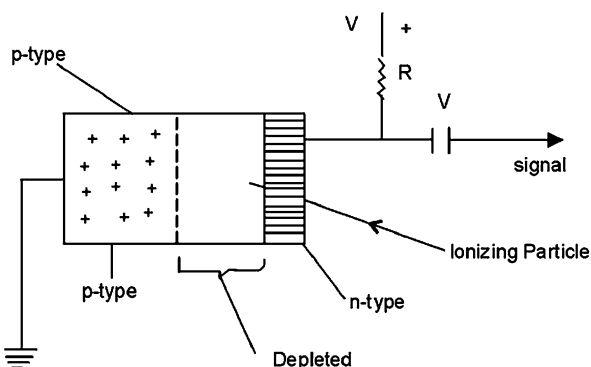
*Example 1.9* A G.M. tube with a cathode and anode of 2 cm and 0.12 mm radii, respectively is filled with Argon gas to 10 cm Hg pressure. If the tube has 1.2 kV applied across it, estimate the distance from the anode, at which electron gains just enough energy in one mean free path to ionize Argon. Ionization potential of Argon is 15.7 eV and mean free path in Argon is  $2 \times 10^{-4}$  cm at 76 cm Hg pressure.

**Solution** Since the mean free path is inversely proportional to pressure, M.F.P at 10 cm pressure will be  $2 \times 10^{-4} \times (76/10)$  or  $1.52 \times 10^{-3}$  cm.

The electric field at a distance = M.F.P, should be such that it acquires just sufficient energy to ionize Argon (15.7 eV). The required value of  $E$  is

$$\begin{aligned} E &= \frac{15.7}{1.52 \times 10^{-3}} = 1.03 \times 10^4 \text{ volt/cm} \\ r &= \frac{V}{E \ln(b/a)} = \frac{1200}{1.03 \times 10^4 \ln(20/0.12)} \\ &= 0.0227 \text{ cm} \quad \text{or} \\ &= 0.227 \text{ mm} \end{aligned}$$

**Fig. 1.11** A typical silicon depletion layer detector. A negative pulse appears across  $R$



## 1.7 Semi-conductor Particle Detectors

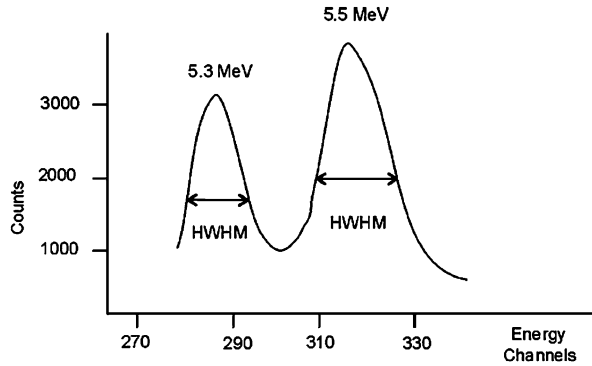
### 1.7.1 Resolution

In gases incident charged particles produce negatively charged electrons and positively charged ions, whereas in semi-conductors they produce free  $e^-$  and positively charged “holes”. Second difference is that in silicon a charged particle will produce one electron-hole pair for each 3.5 eV absorbed. This is an order of magnitude smaller than the corresponding value in a gas ( $\sim 35$  eV). This leads to the production of ten times the number of carrier pairs, and therefore smaller relative straggling for the recorded particles. Thus, more accurate energy measurements can be made. A 5 MeV particle stopping in silicon releases  $1.43 \times 10^6$  electron-hole pairs with a S.D.  $= \pm 1.2 \times 10^3$  or relative S.D.  $(\sigma/m) = 0.08\%$ . Limiting fluctuation for gas ionization chamber is  $\pm 0.23\%$  and is approximately 0.8% for scintillation detector. Theoretical resolution is not achieved because of electronic noise in the semiconductor detector and its associated pre-amplifier and for inefficient charge collection. Thus, semiconductor detectors are preferred where energy resolution is important.

### 1.7.2 Reversed Biased p-n Junction Particle Detector

Figure 1.11 is a diagrammatic representation of a silicon depletion-layer detector. The p-type silicon contains an excess of acceptor impurities so that there are more holes than free electrons and is reversed biased. It occupies the main body of the detector. The n-type silicon is made extremely thin, usually about  $0.1 \mu\text{m}$ . It is heavily doped with a donor and this region contains high concentration of free electrons and practically no free holes. The thickness of the depletion layer ranges from  $10 \mu\text{m}$  to 5 mm, depending upon the detector construction and the value of the applied voltage. Since the n-type region is so thin that the p-n junction may be considered to be on the surface for all practical purposes. Hence this type of detector is also called surface barrier detector. A typical surface barrier detector for alpha-particle

**Fig. 1.12** Alpha energy spectrum from a composite source obtained from the silicon surface barrier detector



measurements may have a depletion layer of 100  $\mu\text{m}$  with an applied potential of 100 volts. Sensitive areas of 2–3  $\text{cm}^2$  or larger are available. When a reverse bias voltage is applied as in Fig. 1.11, the depletion layer contains neither free electrons nor holes. Under these conditions, current flow through the device is severely limited. A charged particle or gamma ray that passes through the depletion layer of the junction, generates electron-hole pairs which drift to the opposite sides of the junction under the action of a reverse bias potential and result in a fast voltage pulse ( $\sim 10^{-8}$  sec). An upper limit for the carrier velocities is  $\sim 10^7$  cm/sec, and this together with the depletion layer thickness, sets a lower limit for the charge collection time. The magnitude of the pulse is proportional to energy lost by the incident particle crossing the thin junction region.

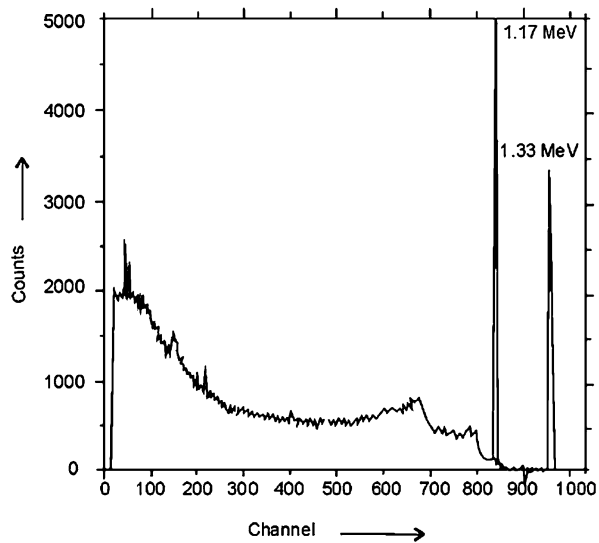
From the point of view of noise, the field effect transistor (FET) in the first stage of the amplifier is the best electronic device and it limits the resolution by itself to approximately 60 eV. The energy spectrum of radiation can be obtained using a pulse height analyzer, as in the case of scintillation counter.

Very thin transmission detectors give a signal proportional to  $dE/dx$ , while total absorption of the particle gives  $E$ . The combination of the two signals permits the identity of particles generating them. Figure 1.12 shows the alpha energy spectrum of a composite source consisting of  $^{210}\text{Po}$  and  $^{238}\text{Pu}$  obtained from a silicon barrier layer detector and a pulse height analyzer. The half-width at half maximum (HWHM) is measured on the higher side of the peaks to minimize the effects of finite source thickness.

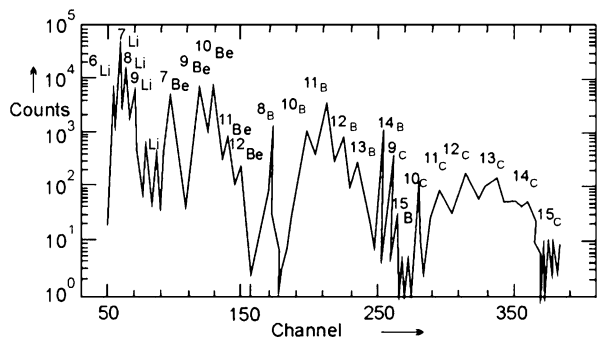
Figure 1.13 shows the gamma-ray spectrum from  $^{60}\text{Co}$  observed by a germanium detector. The photo peaks due to 1.17 MeV and 1.33 MeV are indicated. The Compton shoulders as well as the sharp drops in the curve at channel No: 680 and No: 790 which are Compton edges corresponding to maximum transfer of energy to electrons are also shown.

Figure 1.14 shows the mass separation for the fragments produced in the collisions of 5 GeV protons with the nuclei of Uranium. Each product particle is passed through a thin silicon detector for  $dE/dx$  measurement and stopped in the second detector for  $E$  measurement. The two signals are combined in coincidence to permit the product nuclei to be identified. The mass spectrum also shows the first observation of the short lived isotopes  $^{11}\text{Li}$ ,  $^{14}\text{B}$  and  $^{15}\text{B}$ .

**Fig. 1.13** Gamma-ray spectrum due to 1.17 MeV and 1.33 MeV from  $^{60}\text{Co}$  [1]



**Fig. 1.14** The mass spectrum of isotopes produced in fragmentation of Uranium nuclei by 5 GeV protons obtained by a detector telescope and particle identifier [1]



### 1.7.3 Advantages

- i. These detectors have excellent energy resolution.
- ii. Their energy response is linear over a wide range of particles and energies.
- iii. The pulse rise time in these detectors is short, being of the order of  $10^{-8}$  sec. These features make them suitable for Nuclear Spectroscopy, which includes nuclear product separation, Neutron spectroscopy, Beta spectroscopy, Gamma-ray spectroscopy and Fission studies.
- iv. The output is insensitive to counting rate.
- v. They involve substantially windowless operation. This means that low energy particles can easily enter the sensitive region.
- vi. They have variable sensitive thickness.
- vii. Unlike scintillation counters, they are insensitive to magnetic fields.
- viii. They involve low temperature operation.

- ix. Their small size, low cost and low power requirements make them amenable for space applications.

### ***1.7.4 Applications***

- i. These detectors have a decisive advantage in Nuclear reaction charged particle spectroscopy and in mass separation specially when heavy energetic particles must be measured in the presence of a heavy background of light particles of high energies.
- ii. The insensitivity of silicon semiconductor detectors to low energy neutrons and gamma-radiation has been of tremendous importance in fission studies. This property has permitted their use in a thermal-neutron flux of about  $10^9$  neutrons  $\text{cm}^{-2} \text{sec}^{-1}$  for investigations of correlated fission kinetic energies.
- iii. Neutron sensitivity in a few MeV region has been achieved in two ways
  - (a) by detecting recoil protons from a hydrogenous radiator and
  - (b) by detecting charged particles produced in suitable neutron induced reactions. The other possibility is to diffuse  $^{10}\text{B}$  inside silicon and exploit the reaction  $^{10}\text{B}(n, \alpha) ^7\text{Li}$ .
- iv. In beta-spectroscopy, the low atomic number of silicon has the advantage of reducing the backscattering.
- v. For Gamma-ray spectroscopy the low atomic number of silicon together with the small sensitive volume of semi conductor detector results in a low detection efficiency for gamma rays. However, in applications which require good energy resolution of relatively low energy gamma rays where high detection efficiency is not of great importance, the use of germanium rather than silicon has proved very useful. A line width of 9.0 keV from 660 keV gamma-rays of  $^{137}\text{Cs}$  has been obtained.
- vi. Semiconductor detectors can detect minimum ionizing particles since the rate of loss of energy of a singly charged minimum ionizing particles in silicon is  $\cong 400$  keV/mm and it is possible to use devices with several mm sensitive thickness.
- vii. Properties of semiconductors like energy requirement of electron-hole pairs in silicon and germanium, the electron multiplication phenomenon in germanium and silicon, and photo-conductive processes in germanium, carrier life times, carrier diffusion lengths and carrier capture cross section have been determined from the well defined amount of charge liberated by monoenergetic beams of protons and of  $\alpha$ 's of different energies.

### ***1.7.5 Disadvantages***

- i. Long range particles are not stopped.
- ii. These devices have short operating life time

- iii. The output signal is small
- iv. The devices can not be operated at high temperatures
- v. The counting behavior changes due to radiation damages.
- vi. There is a change of characteristics with different ambient for some of the detectors.

*Example 1.10* A depletion-layer detector has an electrical capacitance determined by the thickness of the insulating dielectric. Estimate the capacitance of a silicon detector with the following characteristics: area  $1.6 \text{ cm}^2$ , dielectric constant 11, depletion layer  $45 \text{ }\mu\text{m}$ . What potential will be developed across this capacitance by the absorption of a  $4.5 \text{ MeV}$  alpha particle which produces one ion pair for each  $3.5 \text{ eV}$  dissipated?

### Solution

$$C = \frac{\epsilon AK}{d} = \frac{8.8 \times 10^{-12} \times 1.6 \times 10^{-4} \times 11}{45 \times 10^{-6}} = 344 \times 10^{-12} \text{ F}$$

$$q = \frac{4.5 \times 10^6 \times 1.6 \times 10^{-19}}{3.5} = 2.06 \times 10^{-13} \text{ coulomb}$$

$$V = \frac{q}{C} = \frac{2.06 \times 10^{-13}}{344 \times 10^{-12}} = 6 \times 10^{-4} \text{ volts}$$

## 1.8 Neutron Detectors

### 1.8.1 Principle

Neutrons being neutral cannot be detected directly. They can be detected only by means of secondary charged particles which are released in their nuclear reactions or scattering which they undergo in passing through matter. The secondary particles must be produced at energies which can produce ionization and which can be detected. The secondary charged particles could be protons recoiling in the collision of neutrons with hydrogen nuclei or they may be the products of nuclear reactions induced by neutrons with nuclei of suitable targets. One or more charged particles are emitted. Exothermic reactions  $(n, p)$ ,  $(n, \alpha)$ ,  $(n, f)$  and  $(n, \gamma)$  are suitable as they have large cross sections for slow neutrons ( $\sigma \propto 1/v$ ). A typical example is the reaction



Alternatively, the secondary particles could be the radiations from radioactive product nuclei formed as the result of neutron capture. The detection of neutrons is dictated by the requirement that measurable ionization effects be produced.

## 1.8.2 Desired Characteristics of Neutron Detectors

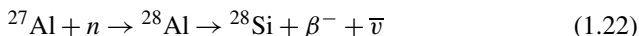
- i. The detection efficiency must be high.
- ii. Neutron capture cross section must be large, so also the Q-value of nuclear reaction.
- iii. Other competitive reactions must have negligible rates.
- iv. In the time-of-flight method, detector must have high detection efficiency and fast rise time of pulses. Organic scintillators serving both as proton target and as a proton detector are commonly used for such applications.

Slow neutrons on collision with hydrogen nuclei will not produce protons which would generate enough ionization. Also, fast neutrons often do not have high capture cross-section to induce nuclear reactions or to produce radioactive nuclei. Consequently, detection can be classified to a large extent in terms of the energy of the neutrons.

## 1.8.3 Slow Neutron Detectors

### 1.8.3.1 Foil Activation Method

Numerous nuclides have a large activation cross section for  $(n, \gamma)$  reaction at low neutron energy. In this method, a thin foil of the given material is exposed to neutrons of known intensity and the induced radioactivity is determined. Consider, for example, the absorption of thermal neutrons by  $^{27}\text{Al}$  to form 2.3 min  $^{28}\text{Al}$  according to



If the thickness of the foil is small so that radiation intensity may be assumed constant across the material, then considering 1 cm area of the foil that is exposed

$$\frac{\Delta I}{\Delta x} = I \Sigma_\alpha \quad (1.23)$$

where  $I$  is the initial beam intensity,  $\Sigma_\alpha$  is the macroscopic absorption cross section. But for each neutron lost from the beam, one atom of  $^{28}\text{Al}$  is formed and since the volume of aluminum is  $\Delta x \times 1^2$  or  $\Delta x \text{ cm}^3$ ,

$$\text{Interactions/cm}^3/\text{sec} = I \Sigma_\alpha \quad (1.24)$$

As soon as  $^{28}\text{Al}$  is formed, it will start decaying at a rate determined by its decay constant  $\lambda$ . If  $Q$  is the number of atoms of  $^{28}\text{Al}$  present at any time  $t$ ,

$$(\text{Net rate of change of } Q) = (\text{Production rate}) - (\text{Decay rate})$$

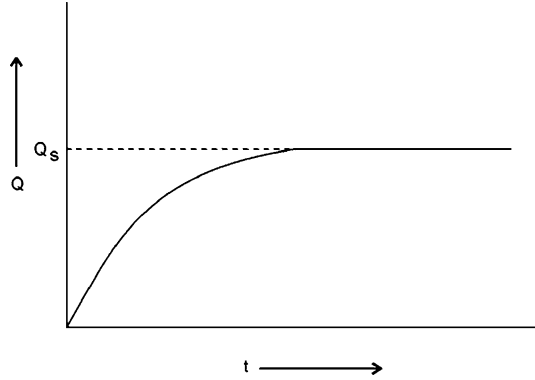
$$\frac{dQ}{dt} = I \Sigma_\alpha - \lambda Q \quad (1.25)$$

$$t = \int dt = \int \frac{dQ}{I \Sigma_\alpha - \lambda Q} + C \quad (1.26)$$

where  $C$  is the constant of integration.



**Fig. 1.15** Number of  $^{28}\text{Al}$  atoms as a function of time



Solving (1.26) with the condition that  $Q = 0$  at  $t = 0$ , we easily find,

$$Q = \frac{I \Sigma_a}{\lambda} (1 - e^{-\lambda t}) \quad (1.27)$$

After a time much longer than say 5 times  $1/\lambda$ , the exponential term tends to zero, and

$$Q \rightarrow Q_s = \frac{I \Sigma_a}{\lambda} \quad (1.28)$$

$Q_s$  represents the saturation value, Fig. 1.15. At this time and beyond,  $dQ/dt = 0$  as is evident by substituting (1.28) in (1.25), i.e. Rate of production = Rate of decay.

After this state of affairs is reached, the foil is removed and after the lapse of known time  $t_w$  (called waiting time), the radioactivity is measured. Then

$$Q = Q_s e^{-t_w \lambda} \quad (1.29)$$

and

$$\left| \frac{dQ}{dt} \right| = \lambda Q = \lambda Q_s e^{-t_w \lambda} = I \Sigma_a e^{-t_w \lambda} \quad (1.30)$$

knowing the value of  $\Sigma_a$ , intensity of neutrons  $I$  can be determined.

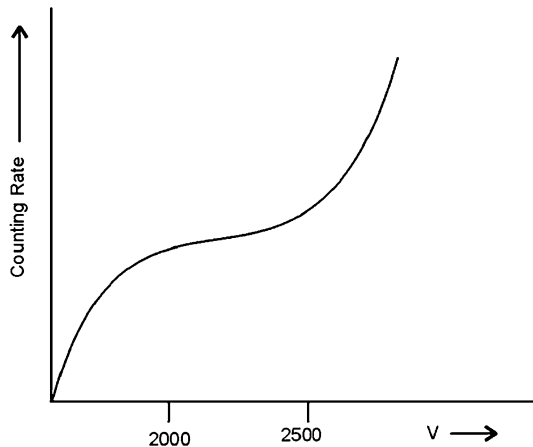
### 1.8.3.2 Boron Detectors

#### BF<sub>3</sub> (Boron-Trifluoride) Proportional Counters

A counter or an ionization chamber filled with BF<sub>3</sub> gas can detect neutrons through reaction (1.21). The gas serves the purpose of both target material as well as the medium in which charged product nuclei may be arrested. BF<sub>3</sub> counters like other proportional counters are fabricated in cylindrical geometry. The outer tube acts as a cathode and the central wire as the anode. Operating voltage is usually 2000–2500 V, Fig. 1.16. Typical values of the gas multiplication are 100 to 500. BF<sub>3</sub> counter can discriminate thermal neutron induced pulses against those induced by gamma rays.

If a thermal neutron is absorbed by  $^{10}\text{B}$  nucleus, about 2.3 MeV appears as kinetic energy of  $\alpha$  and the recoiling nucleus  $^7\text{Li}$ . If the counter is operated in the

**Fig. 1.16** Characteristics of  $\text{BF}_3$  counter



proportional region, it is possible to count the large pulses against a heavy background of smaller pulses due to  $\gamma$  rays. Assume a speed distribution  $n_v$  such that there are no neutrons outside the  $1/v$  limit for boron, i.e.  $E > 1$  keV. The product  $n_v dv$  is the number of neutrons/unit volume with speeds between  $v$  and  $v + dv$ . If  $N_0$  is the number of boron nuclei in the counter there is a contribution  $dR$  to the detector counting rate of

$$dR = \sigma N_0 n_v v dv \quad (1.31)$$

The total detector counting rate is

$$R = \int \sigma N_0 n_v v dv = \sigma v N_0 \int n_v dv \quad (1.32)$$

as  $(\sigma v)$  is independent of  $v$ . Also, the last integral in (1.32) represents  $n$ , the neutron density regardless of speed

$$R = N_0 n (\sigma v) \quad (1.33)$$

A thin boron detector then gives an output proportional to the neutron density. This is true either for a collimated beam or an isotropic flux.

### Boron Lined Proportional Counters

The counter is lined with a boron compound, and filled with a suitable gas. Only one of the particles deposits energy in the counter gas. These counters show less satisfactory plateau.

#### 1.8.3.3 $^3\text{He}$ Proportional Counters

These counters use  $^3\text{He}$  ( $n, p$ ) $^3\text{H}$  reaction. The absorption cross section is large ( $\sigma = 5327$  barns) for thermal neutrons and the  $Q$ -value of 0.77 MeV is favourable.

Further Helium is a good filling gas for proportional counters. These features make  $^3\text{He}$  ( $n, p$ )  $^3\text{H}$  reaction quite attractive both for neutron counting and spectrometry.

### 1.8.4 Fission Detectors

Fission reactions induced by slow and thermal neutrons in the nuclei of  $^{235}\text{U}$ ,  $^{233}\text{U}$  and  $^{239}\text{Pu}$  are quite suitable for neutron detection. When the fissile elements are used in the proportional counters, because of large energy that is released (170 MeV) they provide a good discrimination against alphas from natural radioactivity.

### 1.8.5 Fast Neutron Detectors

The activation cross section of most nuclides is quite small for neutrons of energy greater than 1 MeV so that the activation method or the use of neutron induced nuclear reaction detectors is ruled out. However, the observation of recoil protons in  $n-p$  scattering furnishes a method for neutron detection. First the scattering cross sections for  $n-p$  scattering are reasonably large, being 4 barns at 1 MeV neutron energy and 1 barn at 10 MeV energy. An organic scintillation counter is a suitable detector. Under the assumption that  $n-p$  scattering is isotropic in the C.M. system, it can be shown that the recoil protons in the Lab system have a uniform distribution.

$$\frac{d\sigma}{d\omega^*} = \frac{\sigma}{4\pi} \quad (1.34)$$

$$\frac{d\sigma}{dE_p} = \frac{d\sigma}{d\omega^*} \cdot \frac{d\omega^*}{dE_p} = \frac{\sigma}{4\pi} \cdot \frac{2\pi \sin\phi^* d\phi^*}{dE_p} \quad (1.35)$$

where quantities with \* refer to CMS. But

$$\phi^* = 2\phi \quad \text{and} \quad d\phi^* = 2d\phi \quad (1.36)$$

If  $E_0$  is the initial neutron energy in the Lab system,

$$P_0^2 = 2ME_0$$

The momentum of the recoil proton  $P_p$  is given by

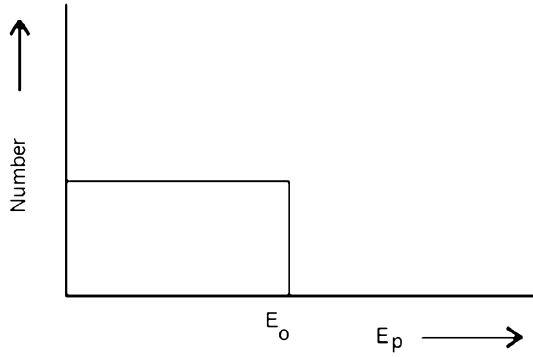
$$\begin{aligned} P_p &= P_0 \cos\phi \\ P_p^2 &= P_0^2 \cos^2\phi \\ E_p &= E_0 \cos^2\phi \\ dE_p &= 2E_0 \cos\phi \sin\phi d\phi \end{aligned} \quad (1.37)$$

where we have ignored the negative sign in (1.37) as  $E_p$  decreases when  $\phi$  increases.

Using (1.36) and (1.37) in (1.35) and simplifying

$$\frac{d\sigma}{dE_p} = \frac{\sigma}{E_0} = \text{const.} \quad (1.38)$$

**Fig. 1.17** Energy distribution of recoil protons



Equation (1.38) shows that the recoil energy of protons is uniform, Fig. 1.17, the proton energy ranging from 0 to  $E_0$  for  $\phi = 90^\circ$  to  $\phi = 0$ . The number of proton recoils per sec in the energy.

Interval  $E$  and  $E + dE$  is

$$d\sigma = \frac{\sigma}{E_0} N_0 \phi dE_p \quad (1.39)$$

where  $N_0$  = total number of atoms in the chamber and  $\phi$  is the flux of neutrons. Knowing  $d\sigma/dE_p$  and  $\sigma$ , the flux  $\phi$  can be determined.

### 1.8.6 Transmission Experiments

Neutrons disappear from collimated beams like “One shot” process similar to gamma rays, the intensity decreasing exponentially with distance in the medium. The absorption coefficient  $\mu$  can be determined. This is simply the macroscopic cross section.

*Example 1.11*  $^{60}\text{Co}$  is produced from natural cobalt in a reactor with a thermal neutron flux density of  $2 \times 10^{12} \text{ n cm}^{-2} \text{ sec}^{-1}$ . Determine the maximum specific activity. Given  $\sigma_{act} = 20$  barns.

**Solution**  $Q_{\max} = \frac{\phi \Sigma_{act}}{\lambda} = \frac{\phi \sigma_a}{\lambda} \cdot \frac{N_{(av)}}{A}$

$$\begin{aligned} \left| \frac{dQ}{dt} \right| &= Q_{\max} \lambda = \frac{\phi \sigma_{act} N_{(av)}}{A} = \frac{2 \times 10^{12} \times 20 \times 10^{-24} \times 6 \times 10^{23}}{60} \\ &= 4 \times 10^{11} \text{ D.P. s} \\ &= \frac{4 \times 10^{11}}{3.7 \times 10^{10}} \text{ Ci} \\ &= 11 \text{ Ci} \end{aligned}$$

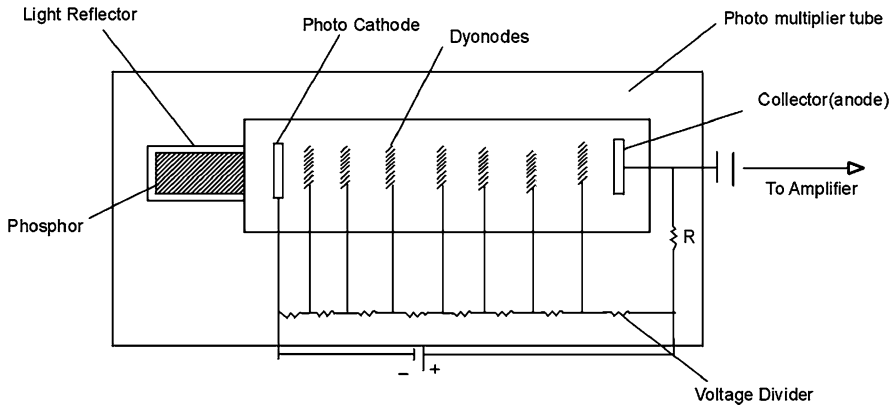


**Fig. 1.18** Block diagram of a scintillation counter

**Example 1.12** Natural cobalt is irradiated in a reactor with a thermal neutron flux density of  $4 \times 10^{12} n \text{ cm}^{-2} \text{ sec}^{-1}$ . How long an irradiation will be required to reach 25 % of the maximum activity? Given  $T_{1/2} = 5.3$  years.

**Solution**  $\left| \frac{dQ}{dt} \right| = Q\lambda = \varphi \Sigma_{act} (1 - e^{-\lambda t})$

$$\frac{Q}{Q_s} = \frac{25}{100} = (1 - e^{-0.693t/5.3})$$

Solving for  $t$ , we find  $t = 2.2$  years.

## 1.9 Scintillation Counter

### 1.9.1 Construction

Figure 1.18 is a representative diagram of a scintillation counter. It consists of a photomultiplier tube to which is fixed a scintillator. A high voltage (of the order of a kV) is applied between the photo-cathode and the anode. The dynodes incorporated in the tube produce electron multiplication and by the use of a voltage divider provide progressively larger voltage between cathode and anode. Scintillators exist in several forms, crystals (organic or inorganic), liquids, plastic solids and gases. The scintillation phenomenon depends on the fact that suitable “fluors” give off pulses of light when traversed by a charged particle. This light is directed on to a photo-multiplier cathode where it ejects electrons by photo-electric effect. These electrons are multiplied in the dynode structure of the tube. In each stage the number of secondary electrons is multiplied which are finally collected at the anode and recorded as a pulse by suitable circuits. The phosphor is in optical contact with the tube and is protected from external light. A reflector surrounding the phosphor enhances light falling on the photo-cathode for higher efficiency.

### ***1.9.2 Mechanism***

A charged particle passing through the phosphor loses energy by ionization, excitation and dissociation of molecules close to its path, ultimately light is emitted. The solid phosphor can be basically divided into

- i. organic
- ii. inorganic crystals.

There are several important differences between the characteristics of organic and inorganic scintillators, in regard to lifetimes, linearity of energy response, temperature effects, fluorescence and conversion efficiency and  $\nu_{\max}$  at which maximum number of photons are emitted. The basic difference in the mechanism for the light production is that light emitted by an inorganic crystal is primarily due to the crystal structure, where as organic substances exhibit luminescence by virtue of molecular properties.

### ***1.9.3 Desirable Characteristics of Luminescent Materials***

- i. The phosphor must have high efficiency for conversion of incident energy of radiation or particles into that of the emitted luminescence. In the case of inorganic phosphor material a small percentage impurity is essential while for organic phosphors, material must be pure.
- ii. The spectrum of the emitted light must closely match the spectral response of the cathode of the photomultiplier used (in the blue, violet or u.v. region).
- iii. The luminescent material must be transparent to their own luminescence radiation.
- iv. The material used must be a large optically homogeneous mass, either as a single crystal without defects or in solution, solid or liquid, moulded or machined to any convenient shape.
- v. The phosphor must have a high stopping power for the radiation to be detected.
- vi. The rise and decay of luminescence during and after excitation should occur in a short time.
- vii. The phosphor must be stable against vacuum conditions and under prolonged irradiation.
- viii. The refractive index  $\mu$  of the crystal should not be too high, otherwise light will not be able to come out easily due to internal reflections.

### ***1.9.4 Organic Scintillators***

- i. In organic scintillators, the main mechanism is believed to be that of collisions which are responsible for the energy transfer from the molecules, either by excitation transfer or by a dipole resonance interaction

- ii. The energy response, i.e. light output as a function of energy loss of particle, is not quite linear. Light output is very much dependent upon the nature of the particle.
- iii. Organic scintillators have lifetimes of the order of  $10^{-9}$  to  $10^{-8}$  sec.
- iv. The phenomenon of phosphorescence is absent.
- v. The fluorescent conversion efficiency is generally smaller than the inorganic phosphors, conversion efficiency of anthracene is about half that of sodium iodide.
- vi. Suitable organic scintillators are anthracene, ( $\lambda_{\max} = 4400 \text{ \AA}$ ), diphenylacetylene, terphenyl naphthalene and stilbene. Among plastics, anthracene in polystyrene is found to be useful. Terephenyl in toluene and terphenyl in xylene are good liquid organic scintillators.
- vii. Organic phosphors are extensively used for fast neutron detection. The interactions of fast neutrons with hydrogen produce fast recoil protons which can be detected with high efficiency in large crystals.

### 1.9.5 Inorganic Scintillators

- i. In inorganic crystals, for example alkali halides notably NaI with thallium impurity, charged particles may raise electrons into the conduction bands or into excitation levels. The electron and the hole left move rapidly through out the crystal as an exciton until captured by the imperfection, giving up the energy in the form of vibrational transfer or until captured by an impurity. The impurity gets excited and acts as a scintillator. In the case of halides, thallium is added as an impurity to the extent of 0.1 to 0.2 percent. These crystals are highly transparent to their own radiation.
- ii. The light output from inorganic crystals like NaI is very nearly proportional to energy loss down to about 1 MeV for protons and about 15 MeV for  $\alpha$ 's.
- iii. The life times of inorganic scintillators are generally longer than those of organic scintillators, being of the order of  $10^{-6}$  sec.
- iv. The phenomenon of phosphorescence which is delayed emission of photons can in certain cases cause generation of secondary pulses which are indistinguishable from the primary pulses. As sodium iodide is deliquescent, it must be protected from moisture; nevertheless it is the most widely used inorganic phosphor. Large size crystals up to several inches in diameter and length are available. It has a high density and contains high  $Z$  atoms of Iodine and is an efficient detector for gamma rays as the absorption cross section for the three important processes, photoelectric, Compton and pair-production vary as  $Z^{4.5}$ ,  $Z$  and  $Z^2$  respectively. Of the other inorganic phosphors, zinc sulphide is useful for alpha-particle detection and lithium iodide for neutron detection, the relevant nuclear reaction being



- v. Important inorganic scintillators are, sodium iodide (thallium activated,  $\lambda_{\max}$  being 4100 Å), cesium iodide (cooled to 77 K), zinc sulphide (copper activated) and lithium iodide (europium activated).
- vi. Some of the inorganic phosphors have a high value of the refractive index ( $\sim 2$ ). Difficulty is experienced in getting light out of them.

### ***1.9.6 Photo-Multiplier (PM) Characteristics***

The desired characteristics of Photo-multiplier (PM) are:

- i. PM must have a photo cathode of large cathode area with an end-window.
- ii. PM must be of a high efficiency for converting photons into photo-electrons. A peak of conversion efficiency in the blue or ultra violet region is desirable.
- iii. PM must provide a high gain.
- iv. It must provide a good signal-to-noise ratio. In the absence of light the output from a photomultiplier consists of numerous pulses (noise) of various sizes, principally due to thermal emission of electrons from the photo-cathode. This constitutes the so-called dark current which depends on the photo-cathode material. It can be reduced by cooling the cathode. Popular photomultipliers are 56 AVP (Philips), 6810 A, 7264 (RCA), 6292 Du Mont. The number of dynodes varies normally from 10 to 15.

### ***1.9.7 Light Collection***

A crystal scintillation counter is normally placed in a metal container. When hygroscopic alkali halides are used, they are protected against moisture by sealing the container. Good optical contact is made between the surface of phosphor and the end face of PM with a layer of clear vacuum grease and by placing a good reflector in optical contact with other crystal surfaces so that light which would otherwise escape will be returned to the photomultiplier with improved efficiency. A highly polished foil or a diffuse reflector such as magnesium oxide is used as a specular reflector. When the arrangement is such that the PM can not be in direct contact with the scintillator, lucite pipes can be used.

### ***1.9.8 Background***

The background of an unshielded scintillator arises due to three major sources:

- i.  $\gamma$ -radioactivity in the neighborhood, which can be reduced by shielding the counter.



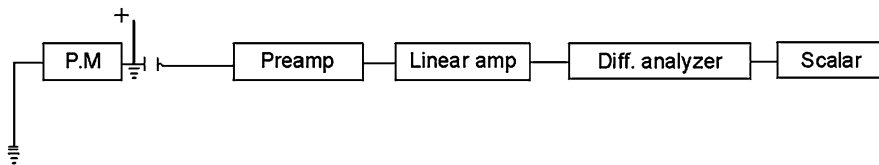


**Fig. 1.19** Block diagram of electronic accessories connected to the PM

- ii. Cosmic rays and other external sources such as reactor or accelerator, if any. This background is reduced by surrounding the scintillation counter with a set of GM tubes, the output of which is arranged in anti-coincidence with the output of the scintillation counter.
- iii. The background noise normally is about 1 per sec for a pulse height equivalent to liberation of 8 photo electrons. This corresponds to a 5 to 10 keV electron incident on a NaI crystal. This can be reduced by cooling the counter. Alternatively, the phosphor is viewed by two photomultipliers in coincidence. In this case, the noise pulses which occur randomly alone contribute to chance coincidence.

### 1.9.9 Electronic Equipment

Figure 1.19 is a block diagram of the electronic equipment attached to the PM. Pulses from the anode of the PM which are small are passed through a pre-amplifier and then to a linear amplifier and through a “window” of the differential analyzer, and finally counted by the scalar. The high voltage can be varied to suite the given PM. The gain of linear amplifier can be varied so that the input fed to the differential analyzer is within the range of operation. The differential analyzer accepts pulses of height between  $V$  and  $V + \Delta V$ , where  $\Delta V$  is the width of the window. The pulse height is proportional to  $E_\gamma$ .

### 1.9.10 Gamma Ray Spectroscopy with NaI (TL) Scintillator

At low  $\gamma$ -ray energy ( $E_\gamma < 100$  keV) photoelectric absorption is the dominating process. As  $\sigma_{ph} \propto Z^{4.5}$ , most of the absorptions occur in Iodine, with the K-shell electron (ionization energy  $E_k = 29$  keV). The vacancy caused by the ejection of electron is filled in by radiative transitions (mainly X-rays) from electrons belonging to upper levels. If the resulting X-rays get absorbed then full energy ( $E_\gamma$ ) is available and this corresponds to photo peak in the pulse height distribution, Fig. 1.20. However, in few events the X-rays escape. Hence energy equal to  $(E_\gamma - E_k)$  is available. This results in the “Iodine escape peak”. The ratio of photons under escape peak to those under photo-peak depends on  $E_\gamma$  crystal size and experimental geometry.

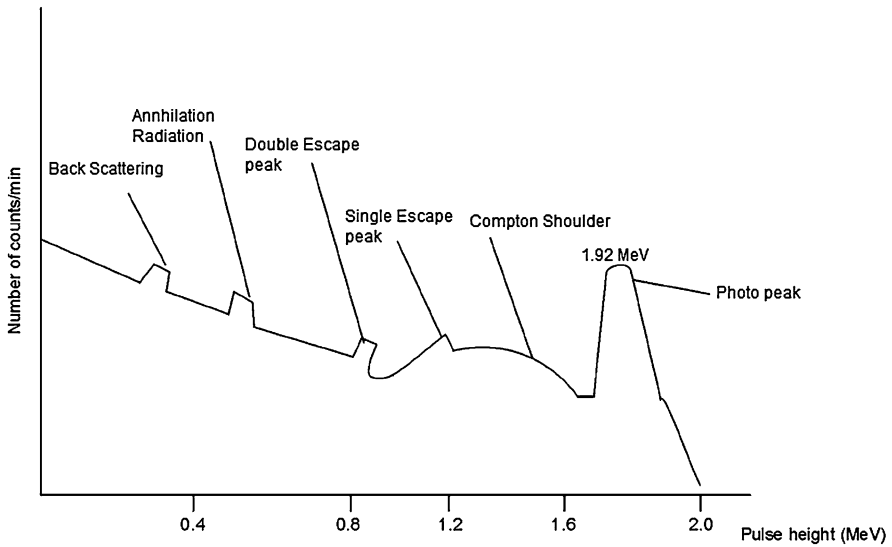


**Fig. 1.20** Pulse height distribution of 3'' x 3'' NaI (TL) showing the positions of various peaks as discussed in the text

For  $E_\gamma > 100$  keV, Compton scattering also becomes significant. The “escape peak” is not significant when the mean absorption length of the incident  $\gamma$ -rays becomes greater than that of iodine X-rays. In the case of single Compton scattering, the energy of escape radiation extends from  $E'$  to  $E_\gamma$ , where  $E' = E_\gamma / (1 + 2\alpha)$  with  $\alpha = E_\gamma / mc^2$  corresponds to the energy of the scattered photon at  $180^\circ$  (back scattering). The corresponding energy deposited ranges from  $(E_\gamma - E')$  to 0. There will be a broad Compton distribution with the Compton edge occurring at energy  $(E_\gamma - E')$ . There can also be external Compton scattering from material outside such as the PM shielding. This gives rise to the “back scattering peak”.

In the case of multiple Compton scattering the energy of escaping radiation extends from 0 to  $E_\gamma$  and the corresponding energy deposited is  $E_\gamma$  to 0. For  $E_\gamma > 2mc^2$  (threshold for pair production) two other peaks are observed, a single escape peak at  $(E_\gamma - mc^2)$  and a double escape peak at  $(E_\gamma - 2mc^2)$ .

Figures 1.21 and 1.22 show typical spectra obtained from  $\gamma$ -rays incident on NaI crystal from Cs-137 (661 keV) and Co-60 (1.17 MeV and 1.33 MeV), respectively.

The 661 keV photo peak, Compton shoulder, back scattering from material of the phosphor and noise are indicated. The decay scheme is also shown.

### 1.9.10.1 Energy Resolution

The photo peaks shown in Figs. 1.21 and 1.22, are not sharp. The energy resolution is defined by the quantity  $\Delta E/E$ , which is the ratio of full width at half maximum to the photon energy. It is important that the spread in photo peaks be as small as

**Fig. 1.21** (a) Pulse height spectrum of  $\gamma$ -rays from Cs-137 of energy 661 keV. (b) Decay scheme for Cs<sup>137</sup>

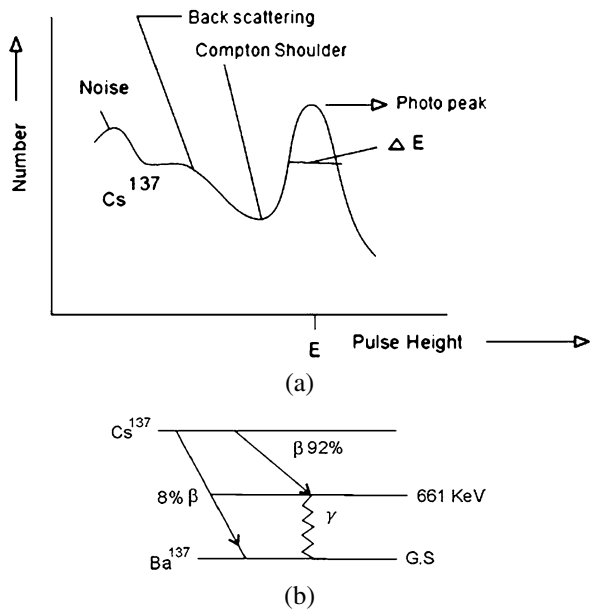
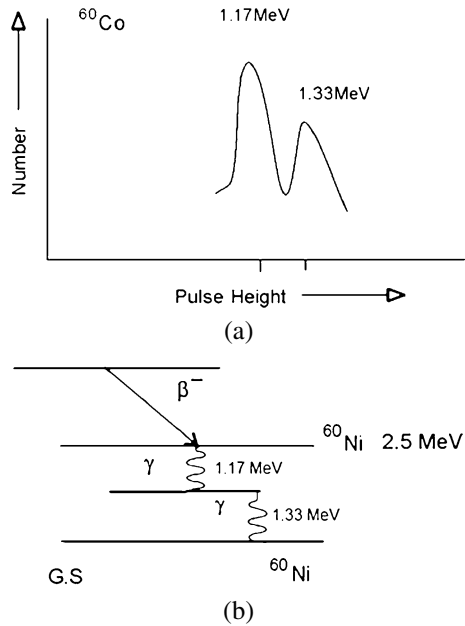


**Fig. 1.22** (a) Pulse height spectrum of  $\gamma$ -rays of energy 1.17 MeV and 1.33 MeV. The origin of  $\gamma$ -rays is shown in the decay scheme. (b) Decay scheme for <sup>60</sup>Co



possible, otherwise  $\gamma$ -rays of neighboring energies cannot be resolved. Many factors contribute to the energy resolution of a scintillation counter. These factors are:

- i. Fluorescent radiation conversion efficiency ( $f$ )
- ii. Efficiency for the collection of light by the cathode ( $b$ )

- iii. Efficiency for the conversion of photo-electrons ( $c$ )
- iv. Efficiency for collection of electrons which are accelerated to the first dynode ( $p$ )
- v. Total multiplication from all the dynodes ( $M$ )

If  $E$  is the particle energy and  $\varepsilon$  the average energy of the photons generated in the crystal, then the number of photons emitted is  $Ef/\varepsilon$ . It follows that the number of electrons finally collected at the output of the PM tube is equal to  $(Ef/\varepsilon)bcpM$ . For various reasons there will be variation in the factors  $f, b, c, p$  and  $M$ . Of various factors, however, the variation in  $c$  which arises due to the statistical fluctuations in the number of photo-electrons released from the photo cathode is decisive for the pulse height and is therefore the ultimate factor which limits the resolution. The best resolution that is achieved is 6 % for 661 keV  $\gamma$ -rays from Cs-137 using NaI phosphor and a 6292 Du Mont P.M. Note that  $\Delta E \propto \sqrt{E_\gamma}$ , so that the energy resolution,  $\Delta E/E \propto 1/\sqrt{E_\gamma}$ .

## 1.9.11 Applications and Advantages

### 1.9.11.1 Fast Timing

For investigations which involve fast timing, the scintillation counters have a decisive advantage over visual detectors. This aspect has been exploited in the lifetime measurements of  $\pi^+$ ,  $K^+$ , capture times of  $\mu^-$  and in the discovery of  $p^-$  by time of flight method. In conjunction with Cerenkov counter or other scintillation counters, it can be used as a “telescope” in coincidence or anti-coincidence to avoid unwanted particles or events (see Chap. 3 for the discovery of  $p^-$ ).

### 1.9.11.2 Scintillation Spectroscopy

Spectrometry of heavy charged particles by scintillation technique is usually done with the use of inorganic crystals. However, a number of organic compounds are also found useful. Organic scintillators like anthracene have a linear response for electrons, but for heavier particles the pulse-height energy relationship exhibit non-linearity. For this reason, organic scintillators are preferred to inorganic crystals for electron spectroscopy as their effective low atomic number causes substantial improvement for backscattering compared with inorganic crystals, except for very low energy electrons.

### 1.9.11.3 Gas Scintillation Counters

Gas scintillation counters have the merit of short decay times ( $\sim 10^{-9}$  s), large light output per MeV independent of ionization density, and their availability in a wide

range of  $Z$  and density. Fission fragments in the presence of heavy background of  $\alpha$ 's can be discriminated. Also, because of low stopping power and small pulse height for  $\gamma$ -rays of nuclear origin, relativistic charged particles can be separated from an intense  $\gamma$  radiation background.

**Example 1.13** Calculate the energy limits of the Compton-scattered photons from annihilation radiation.

**Solution** The energy of annihilation radiation is  $h\nu = m_0c^2 = 511 \text{ keV}$ .

The energy of the scattered photon is

$$h\nu' = \frac{h\nu}{1 + (h\nu/m_0c^2)(1 - \cos\theta)}$$

for  $\theta = 0$ ,

$$h\nu' = h\nu = 511 \text{ keV}$$

for  $\theta = \pi$ ,

$$h\nu' = \frac{h\nu}{3} = \frac{511}{3} = 170 \text{ keV}$$

Thus, the energy limits are 511 keV and 170 keV.

**Example 1.14** A scintillation spectrometer consists of an anthracene crystal and a 10-stage photomultiplier tube. The crystal yields about 15 photons for each 1 keV of energy dissipated. The photo-cathode of the photomultiplier tube generates one photo-electron for every 10 photons striking it, and each dynode produces 3 secondary electrons. Estimate the pulse height observed at the output of the spectrometer if a 1 MeV electron deposits its energy in the crystal. The capacitance of the output circuit is  $1 \times 10^{-10} \text{ F}$ .

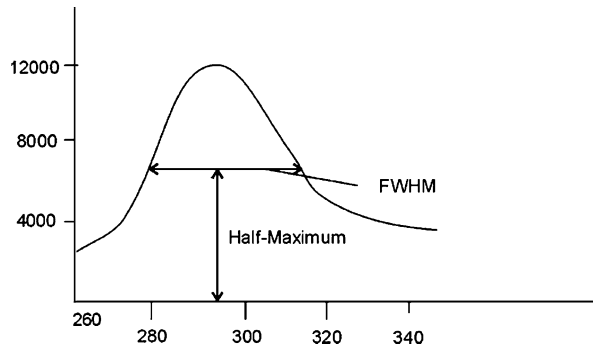
**Solution** Number of photons emitted due to absorption of 1 MeV electron is

$$\frac{15 \times 10^6}{10^3} = 15000$$

Number of photo-electrons emitted =  $\frac{15000}{10} = 1500$ . Since the photomultiplier tube has 10 dynodes and each dynode produces 3 secondary electrons, the electron multiplication factor  $M = 3^{10}$ . The charge collected at the output is  $q = 3^{10} \times 1500 \times 1.6 \times 10^{-19} \text{ Coulomb}$ . The pulse height will be,  $V = \frac{q}{C} = \frac{3^{10} \times 1500 \times 1.6 \times 10^{-19}}{1 \times 10^{-10}} = 0.14 \text{ V}$ .

**Example 1.15** The peak response to the 662-keV gamma rays from  $^{137}\text{Cs}$  shown in Fig. 1.23 occurs in energy channel 298, with half maximum points in channels 281 and 316. Calculate the standard deviation of the energy, assuming the pulse analyzer to be linear.

**Fig. 1.23** Photo peak from 662 keV  $\gamma$ -rays of Cs-137



**Solution** The half width at half maximum,  $\text{HWHM} = 1.177\sigma$ . Full width at half maximum,  $\text{FWHM} = 316 - 281 = 35$ .  $\text{HWHM} = \frac{1}{2}\text{FWHM} = \frac{35}{2} = 17.5$ . The channel 298 corresponds to 662 keV. Hence 17.5 channels correspond to  $\frac{17.5}{298} \times 662 = 38.87$  keV. Standard deviation  $\sigma = \frac{\text{HWHM}}{1.177} = \frac{38.87}{1.177} = 33$  keV.

## 1.10 Cerenkov Counters

Cerenkov counters based on the phenomenon of Cerenkov radiation work in two different modes.

1. The focusing mode which works as a differential mode
2. Non-focusing counter, also known as the threshold counter which detects the presence of particles whose velocities exceed some minimum value.

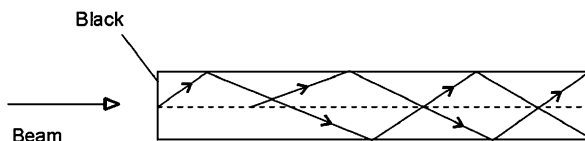
### 1.10.1 Focusing Type (Angular Selection Counters)

In the focusing type the photons in the Cerenkov cone in the angular range  $\theta_1 < \theta < \theta_2$  are selected and directed on to a photomultiplier. It consists of three elements, radiator, focusing system and photomultiplier(s).

#### 1.10.1.1 Radiator

This is the optical medium in which the Cerenkov radiation is produced. The Radiator generally consists of a cylinder of a solid optical medium such as lucite or glass. The cylindrical surfaces and the bases are optically polished. If a fast charged particle does not scatter or interact or appreciably slows down, the unique angle of Cerenkov photons with respect to the axis of the cone is maintained regardless of the number of reflections suffered from the cylindrical surface. The base at the entry is

**Fig. 1.24** Radiator or the generation of Cerenkov radiation



painted black in order to absorb Cerenkov radiation of particles going in the wrong direction, Fig. 1.24.

Liquids in thin cylindrical containers are also used, so also radiators in the pressurized containers. Gas radiators are specially suited for ultra relativistic particles ( $\beta \rightarrow 1$ ) since the refractive index is close to unity. They enjoy a higher velocity resolution  $d\theta/d\beta$ . They also afford the variation of  $\mu$  by simply changing the gas pressure.

### 1.10.1.2 Focusing System

It consists of a series of cylindrical or spherically symmetrical surfaces around the axis parallel to the direction of motion of particle, Fig. 1.25. In practice, two or more photomultipliers generally off the axis are used in coincidence to eliminate accidental coincidences due to tube noise, direct excitations of the photomultiplier by a charged particle, stray light coming from a part of baffle system and due to scattering or inelastic interaction of the incident particle or due to background particles.

### 1.10.1.3 Photomultipliers (PM)

The desirable characteristics of PM are:

- i. Semi-transparent photo cathode of large cathode area be used with an end-window.
- ii. PM must have high efficiency for converting photons into photo-electrons. A peak of conversion efficiency in the blue or ultraviolet is desirable.
- iii. PM must provide high gain.
- iv. It must provide a good signal-to-noise ratio. The dark current due to noise is reduced by cooling the cathode. Popular photomultipliers are 56 AVP (Philips), 6810 A and 7264 (RCA).

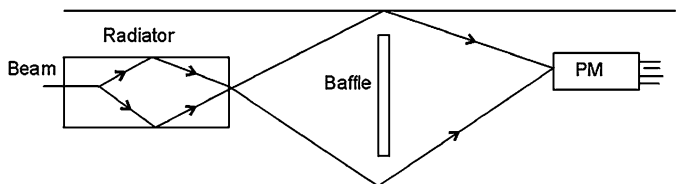


**Fig. 1.25** Focusing system

### 1.10.2 Velocity Resolution [ $\frac{\partial\theta}{\partial\beta}$ ]

$$\cos\theta = \frac{1}{\beta\mu} \quad (1.41)$$

$$\frac{\partial\theta}{\partial\beta} = \frac{1}{\mu\beta^2 \sin\theta} \quad (1.42)$$

For high resolutions,  $\beta \rightarrow 1$  and  $\mu \approx 1$ . It follows that

$$\frac{\partial\theta}{\partial\beta} \cong \frac{1}{\sin\theta} \quad (1.43)$$

However, the intensity,

$$I \sim \text{Const} \cdot \sin^2\theta \quad (1.44)$$

Combining (1.43) and (1.44),

$$\frac{\partial\theta}{\partial\beta} \sim \frac{\text{Const}}{\sqrt{\text{Intensity}}} \quad (1.45)$$

We conclude from (1.43) that a good velocity resolution will be achieved by choosing small  $\theta$  and therefore  $\mu$  close to unity. However, from (1.44) it is obvious that  $\theta$  must be sufficiently larger than zero to permit sufficiently large number of photons to be generated.

### 1.10.3 Non-focusing Counters

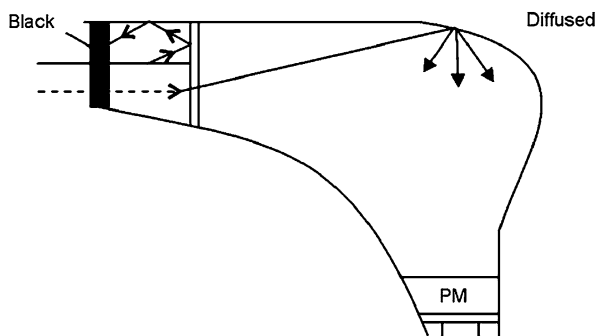
#### 1.10.3.1 Velocity Selectors

A special class of non-focusing counter is used as a velocity interval selecting counter. Here the lower velocity limit is set by the threshold and the upper velocity limit by the internal reflection. Subsequent absorption of light occurs with a cone angle greater than  $\theta_c$ , the critical angle for internal reflection. The back end of the cylindrical radiator is painted black, Fig. 1.26.

This counter is basically used as a last element in a “telescope”. Particles of selected momentum in a magnetic are subjected to a velocity interval selection by requiring a coincidence in a counter with a threshold  $\beta_1$  and an anti coincidence in a counter with a threshold  $\beta_2$ , where  $\beta_2 > \beta_1$ . The velocity range is then defined by  $\beta_1 < \beta < \beta_2$ . Such an arrangement was used in the discovery of antiproton (see Chap. 3).



**Fig. 1.26** Non-focusing counter



### 1.10.4 Total Shower Absorption Cerenkov Counter

These counters use lead loaded glass (density  $4.49 \text{ g/cm}^3$ ,  $\mu = 1.72$ , Radiation length 2 cm) for the radiator element. As the electrons are of several MeV energy, mean number of Cerenkov photons emitted within the radiator is linearly proportional to incident energy. Hence, the mean number of photo-electrons generated at the photo-cathode will be nearly a linear function of the energy of the incident photon or electron.

### 1.10.5 Advantages

**1.10.5.1** All focusing counters are highly directional. Also, non-focusing counters furnish front to back discrimination by painting the back end of the radiator black. Such a method has been used to measure Albedo for cosmic rays in the atmosphere.

**1.10.5.2** As number of Cerenkov photons is proportional to  $z$  at a known velocity, particles of various charges can be separated by the pulse height.

**1.10.5.3** In Cerenkov counters using gas radiator  $\mu$  can be varied by varying pressure of the gas and consequently particles can be selected over a wide range of velocities.

**1.10.5.4** Cerenkov counters can be used to detect short lived particles by placing them close to the source for velocity measurements to avoid intensity losses due to decays. In contrast, in the time of flight method extremely long time of flight paths are involved.

**1.10.5.5** In Cerenkov counters, chance coincidences are enormously reduced compared to scintillation counters.

**1.10.5.6** Cerenkov pulses are extremely fast. Hence jamming of pulses is avoided in contrast with the Scintillation counters in which the decay times for the scintillation process is of the order of  $10^{-9}$  sec.

**1.10.5.7** They eliminate low velocity particles.

### 1.10.6 Disadvantages

**1.10.6.1** Particles can be detected only within a limited direction.

**1.10.6.2** Particles below the threshold velocity can not be detected.

*Example 1.16* What type of material would you choose for a threshold Cerenkov counter which is to be sensitive to 900 MeV/c pions but not to 900 MeV/c protons.

**Solution** Total energy of pion ( $c = 1$ )

$$E_{\pi} = \sqrt{p^2 + m^2} = \sqrt{900^2 + 140^2} = 910.8 \text{ MeV}$$

Pion velocity,  $\beta_{\pi} = \frac{p_{\pi}}{E_{\pi}} = \frac{900}{910.8} = 0.988$ .

For emission at threshold, refractive index

$$\mu_{\pi} = \frac{1}{\beta_{\pi}} = \frac{1}{0.988} = 1.012$$

Total energy of proton

$$E_p = \sqrt{p^2 + m^2} = \sqrt{900^2 + 938^2} = 1300 \text{ MeV}$$

Proton velocity,

$$\beta_p = \frac{p_p}{E_p} = \frac{900}{1300} = 0.692$$

$$\mu_p = \frac{1}{\beta_p} = \frac{1}{0.692} = 1.445$$

Hence the material must have a refractive index in the range  $1.012 < \mu < 1.445$ .

*Example 1.17* Calculate the threshold energy for the production of Cerenkov radiation in Lucite for (a) electron (b) muon (c) proton (d) alpha. The refractive index of lucite is 1.5.

**Solution**

a.

$$\beta = \frac{1}{\mu} = \frac{1}{1.5} = 0.6667$$

$$\gamma = \frac{1}{\sqrt{1 - \beta^2}} = \frac{1}{\sqrt{1 - 0.6667^2}} = 1.3417$$

$$\text{KE(thres)} = (\gamma - 1)m = (1.3417 - 1) \times 0.511$$

$$= 0.1746 \text{ MeV or } 174.6 \text{ keV}$$

b.  $\text{KE(thres)} = (1.3417 - 1) \times 106 = 36.2 \text{ MeV}$

c.  $\text{KE(thres)} = (1.3417 - 1) \times 938 = 320.5 \text{ MeV}$

d.  $\text{KE(thres)} = (1.3417 - 1) \times 3726 = 1273 \text{ MeV}$

## 1.11 Photographic Emulsions

### 1.11.1 Composition

Photographic Emulsions or Nuclear Emulsions differ from ordinary optical emulsions by a higher silver-bromide content, smaller average crystal diameter ( $0.14\text{ }\mu\text{m}$  for  $L_4$  emulsions,  $0.27\text{ }\mu\text{m}$  for  $G_5$  or Nikfi-R emulsions), and much greater thickness. The silver-halide (mainly silver bromide with 5 % silver-iodide) crystals are embedded in gelatin (HCNO). The gelatin is usually made from clippings of calf hide, ear and cheek or from pig skin and bone. The main function of gelatin is to keep the silver halide crystals well dispersed in the medium and to prevent clamping of the crystals. Atomwise, the AgBr group and HCNO groups comprise 25 % and 75 % respectively. But the interactions with medium and high energy particles take place with a frequency of 70 % in AgBr, 20 % in CNO and 5 % in H. The emulsion sheets called pellicles of standard size  $400\text{ }\mu\text{m}$  or  $600\text{ }\mu\text{m}$  are stacked with one on the top of the other before the exposure in order to increase the volume. A variety of emulsions of different crystal sizes have been manufactured which differ in sensitivity. The type  $G_5$ ,  $L_5$  (Ilford), NTB (Kodak), ET-7A (Fuji) and Nikfi-R with crystal size in the range  $0.2\text{ }\mu\text{m}$ – $0.28\text{ }\mu\text{m}$  are highly sensitised and are capable of recording relativistic particles ( $\beta \sim 1$ ).  $K_2$  and  $L_2$  are less sensitised and record protons up to  $\beta = 0.4$ .  $K_1$  is less sensitised and record less protons up to  $\beta = 0.12$ .  $K_0$  is least sensitised and is used mainly for fission studies.

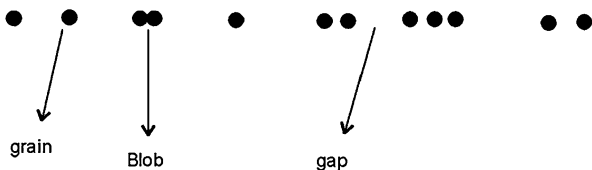
### 1.11.2 Latent Image

When a charged particle moves through emulsion energy is absorbed by the silver halide crystal, and under the action of reducing agent is converted into metallic silver. The physical condition which renders the crystal developable is called “latent image”. The latent image will fade if too much time elapses between irradiation and development, similar to ordinary photography.

### 1.11.3 Processing

Stripped emulsions are first mounted on glass before processing. For uniform development, it is essential that the developer, for example amidol, permeates the thickness of emulsion. For this reason, the plates are bathed in the developer at low temperature ( $0\text{--}5\text{ }^\circ\text{C}$ ) so that the developer is permitted to penetrate but the development will not ensue. Now, if the temperature is raised to say  $23\text{ }^\circ\text{C}$ , the development ensues. This is called high temperature development. After the development stage, the plates are “fixed”, washed and dried in alcohol.

**Fig. 1.27** A typical track in emulsion. Grain, Blob and Gap are indicated



### 1.11.4 Techniques

Events are analyzed with the aid of special type of microscopes with smooth movable stages and high power oil objectives and eyepieces with graticules capable of giving magnifications as high as 2700. After processing, normal emulsion shrinks by a factor of 2–2.5. The shrinkage factor is taken into account in the dip measurements of angles. For particles, which stop within the emulsion stack, Range-Energy-Relation of the type (1-101) is used.

Ionization measurements are made either by counting grains or blobs for relativistic particles or by counting blobs and gaps of length  $> l$ , for non-relativistic particles, and determining the exponent  $g$  from the relation

$$H = B e^{-gl} \quad (1.46)$$

where  $H$  and  $B$  are gap and blob density, respectively. Blobs are unresolved grains and gap is the space separating two successive grains or blobs, as in Fig. 1.27.

For energetic particles, the parameter  $p\beta$  (momentum times velocity) can be found out from multiple scattering measurements by essentially measuring the y-coordinates of the track along the axis, at constant intervals called “cell’s”. The arithmetic average of second differences is given by,

$$\langle |D_2| \rangle = \langle |y_1 - 2y_{i+1} + y_{i+2}| \rangle \quad (1.47)$$

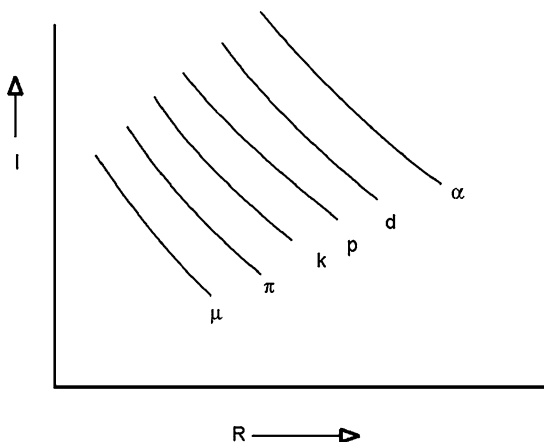
And  $p\beta$  is given by the relation

$$p\beta = \frac{K t^{\frac{3}{2}} \times 18.1}{|D_2|} \quad (1.48)$$

where  $K = 28$  is the scattering constant, for  $\beta > 1$ ,  $D_2$  is in  $\mu\text{m}$ ,  $t$  = cell length in mm and  $p$  in  $\text{GeV}/c$ . The quantity  $t^{\frac{3}{2}}$  arises due to the fact that the scattering angle  $\theta = D/t$ . The factor 18.1 arises due to conversion of degrees into radians. The choice of cell-length is such that the signal-to-noise ratio is greater than 2–3. Multiple scattering technique with constant cell method works provided the energy loss over the tracks is not significant. In order that the method be useful, it is important that the spurious scattering and distortion resulting from the processing of emulsions be small and that the stage noise, which arises due to the non-linear motion of the stage be negligible.

Charge of the particle can be determined from  $\delta$ -ray counting (AAK, 1, 1) or from photometric measurements; for example, the fluxes of heavy primaries of Cosmic rays have been determined from emulsion exposures in balloons or rockets following this procedure.

**Fig. 1.28** Family of curves are obtained for  $I$ - $R$  plots for different particles



Particles are identified from their mass determinations. In this context we recall from (AAK, 1, 1),

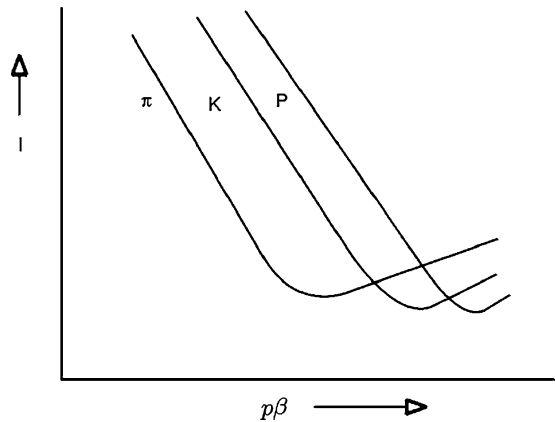
- i. Range measurement gives energy of the particle
- ii. Ionization measurement gives the velocity
- iii. Multiple Scattering measurements give  $p\beta$ .
- iv.  $\delta$ -ray density measurement gives  $z$  of the particle.

For singly charged particles, combination of any two parameters arising in (i), (ii) and (iii) uniquely fixes the mass of the particle since velocity must be eliminated. Thus, the plot of ionization ( $I$ ) versus residual range ( $R$ ) gives a family of curves for particles of different mass, Fig. 1.28. Notice that for the given  $I$ , the ranges are in the ratio of the masses. The method is very extensively used for particles which are brought to rest. Masses can be estimated with an accuracy of about 10 % from a single measurement.

The method can be extended for identifying particles which are not arrested in the emulsion stack, if an appreciable change in ionization over a known distance is determined.

At higher energies, combination of (ii) and (iii) in favorable cases permits the identification of particles, Fig. 1.29. At still higher energies, the curves cross each other and the identification becomes difficult or even impossible. On the other hand, energy measurements can seldom be made from multiple scattering method with an accuracy better than 10–15 % due to the presence of spurious scattering. At energies greater than few GeV, the measurements are rendered meaningless if the noise due to spurious scattering competes with the Coulomb's signal. Sometimes in favorable cases it has been possible to extend the energy measurements up to 15–20 GeV in cosmic ray jets by making relative scattering measurements—a method in which multiple scattering measurements are made with reference to a neighboring track due to an ultra relativistic particle so that spurious scattering and stage noise which affect both the tracks similarly are eliminated.

**Fig. 1.29** Family of curves for the plot of  $I$  vs  $p\beta$  for the particles,  $\pi$ ,  $K$  and  $P$  are shown



### 1.11.5 Advantages

#### 1.11.5.1 High Stopping Power and High Spatial Resolution

Owing to high stopping power, charged particles of moderate energies are easily arrested within the stack of emulsions. Accurate range measurements have permitted precise mass determination of several elementary particles immediately after their discovery. It is usually possible to determine the magnitude and direction of velocity (by blob counting), the rate of change of velocity (by observing variation of Ionization over measured distance), the product of velocity and momentum up to 1.5 GeV/c (from multiple scattering measurements), charge (from delta ray density), the moderation time (from counting number of decays from known traversals and velocity), and the interaction cross-section (from mean free path). Momentum can be measured by bending magnet external to the emulsion, or by employing pulsed magnetic field within the emulsion. Owing to high stopping power a large fraction of even such short-lived particles as hyper fragments and slow  $\Sigma^+$  hyperons are brought to rest before their decay. Their ranges and moderation times are easily measured. In this way reliable measurements of life times of most of the unstable elementary particles have been made in emulsions and also some of the partial decay rates have been evaluated. Because of high spatial resolution time intervals as short as  $10^{-16}$  sec have been measured, a good example being the mean lifetime determination of  $\pi^0$ . Reliable neutron spectroscopy in the energy range, 1–15 MeV is done with the emulsion technique.

#### 1.11.5.2 High Angular Resolution

The angular resolution is unsurpassed. This aspect has been exploited in the determination of the magnetic moment of  $\Lambda^0$ .

### **1.11.5.3 Compactness**

In situations where compactness of equipment is essential, emulsions can be conveniently used. For example, they can be sent in balloons or rockets to high altitudes and recovered conveniently after the required exposure. Further, they are economical.

### **1.11.5.4 Radiation Length**

Because of high stopping power and short radiation length huge electromagnetic cascades can be contained in a large stack and the complete development and final degradation can be studied in detail.

### **1.11.5.5 Loading**

It is possible to load emulsions with  $\text{H}_2\text{O}$ ,  $\text{D}_2\text{O}$ ,  $\text{Li}_2\text{SO}_4$ ,  $\text{Th}(\text{NO}_3)_4$ ,  $\text{UO}_2$  etc. to study reactions with elements which are not contained in normal emulsions.

## ***1.11.6 Limitations***

### **1.11.6.1 Composition Invariability**

The composition of nuclear emulsions can not be changed arbitrarily so that interaction studies are limited only to those nuclei which are present in normal emulsions, although loaded emulsions in limited concentration have been used with some difficulty. The presence of a large variety of nuclei in normal emulsions makes it difficult to identify the target nucleus, although in favorable cases it is possible to identify the groups (Ag, Br, I), (C, N, O), (H), the first one being heavy and the second one light. Events in hydrogen are invariably clean and can be identified confidently.

### **1.11.6.2 Minuteness of Volume**

Because of minuteness of volume of emulsion under study in the microscope it is exceedingly difficult to find correlated events even 1 cm or so apart.

### **1.11.6.3 Continuous Sensitivity**

Because of continuous sensitivity the background tracks are a source of nuisance. The best available emulsions from the stand point of sensitivity lack discrimination and all highly ionizing particle tracks are saturated.

### 1.11.6.4 Distortion and Spurious Scattering

Emulsion which has a gelatin base is subject to distortion in the processing regime. This can seriously affect the range and angle measurements. Spurious scattering can interfere with Coulomb's signal in multiple scattering measurements.

### 1.11.6.5 Scanning

It usually takes several months involving a large group of Physicists and scanners to scan and analyze events of statistical significance.

### 1.11.6.6 The Study of Elementary Interactions

Since only 5 % of the interactions take place with hydrogen and 95 % in complex nuclei of emulsion, the interactions in the latter are obscured by secondary effects. Although hydrogen density in emulsions is comparable with that in hydrogen bubble chamber, the latter is by far better suited in so far as the elementary interaction studies are concerned.

## 1.11.7 Discoveries Made with Photographic Emulsions

The years 1945–54 were the golden era of Nuclear Emulsions. At that time high energy accelerators were not yet available. The only source of high energy particles was in the form of cosmic rays. Major discoveries of fundamental importance included the particles  $\pi^+$ ,  $\pi^-$ ,  $\pi^0$ ,  $K^+$ ,  $K^-$  mesons, several decay modes of  $K^+$  mesons (two-body and three-body decay modes), the hyperons, hyper fragment, double-hyper fragment, the composition of primary cosmic rays etc. Reliable mass measurements of various types of mesons and the  $\Sigma^+$  and  $\Lambda^0$  hyperons, and their mean life times were first carried out in emulsions.

*Example 1.18* The kinetic energy and momentum of a meson deduced from measurements on its track in a nuclear track emulsion are 200 MeV and 490 MeV/c, respectively. Determine the mass of the particle, in terms of the electron mass, and identify it.

### Solution

$$\text{KE} = (\gamma - 1)m = 200 \quad (\text{i})$$

$$P = m\gamma\beta = 490 \quad (\text{ii})$$



where we have put  $c = 1$  and  $\gamma = \frac{1}{\sqrt{1-\beta^2}}$

$$\beta = \frac{\sqrt{\gamma^2 - 1}}{\gamma} \quad (\text{iii})$$

Using (iii) in (ii) and dividing the resultant equation by (i),

$$\frac{\sqrt{\gamma^2 - 1}}{\gamma - 1} = \frac{490}{200} = 2.45$$

or

$$\frac{\sqrt{\gamma + 1}}{\sqrt{\gamma - 1}} = 2.45 \quad (\text{iv})$$

Solving (iv),  $\gamma = 1.4$ . Using the value of  $\gamma$  in (i),  $m = 500 \text{ MeV}/c^2$ .

Mass of meson in terms of electron mass,  $m = \frac{500}{0.511} = 978.5m_e$ .

The particle is a Kaon as its known mass is  $966m_e$ .

## 1.12 Expansion Cloud Chamber

### 1.12.1 Principle

We owe the invention of cloud chamber to C.T.R. Wilson (1912). It contains super-saturated vapor of a gas under pressure. When the chamber is allowed to expand adiabatically, dust particles and preferably ions form nucleation centers around which droplets are formed which grow in size and become visible under proper illumination. If a charged particle passes through the chamber simultaneously a trail of droplets in the form of a track is formed which can be photographed. The unwanted nucleation centres due to dust and the chemical compounds suspended in the gas are removed from the chamber either by electrostatic clearing field or by repeated expansions until dust particles settle on the bottom of the chamber where they stick to the wall.

### 1.12.2 The Stability of Charged Drops

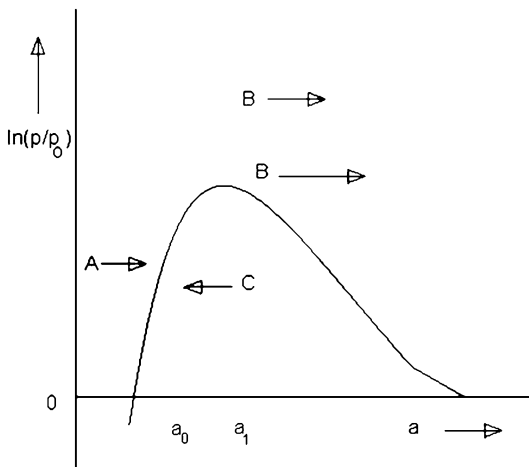
The surface energy of the drop of radius ' $a$ ', surface tension  $S$ , charge  $q$  in an external medium of dielectric constant  $\epsilon_1$  is given by

$$E = 4\pi a^2 S + \frac{1}{2} \frac{q^2}{\epsilon_1 a} \quad (1.49)$$

A change in radius  $a$  results in the change of energy  $\delta E$  and is given by

$$\delta E = \frac{d}{da} \left( 4\pi a^2 S + \frac{1}{2} \frac{q^2}{a \epsilon_1} \right) \delta a \quad (1.50)$$

**Fig. 1.30** Variation of  $\ln(p/p_0)$  with radius of the drop  $a$



This change of energy does not take place in corresponding condensation or evaporation at a plane surface. The change of energy may be equated to the work needed to bring the amount of vapor produced by evaporation at vapor pressure  $p$  in equilibrium with the drop, to the saturation pressure  $p_0$  over a plane surface. We can then write:

$$\frac{d}{da} \left( 4\pi a^2 S + \frac{1}{2} \frac{q^2}{a\epsilon_1} \right) \delta a = 4\pi a^2 p \delta a \frac{R\theta}{M} \ln \frac{P}{P_0} \quad (1.51)$$

where  $\rho$  is the density of the drop,  $\theta$  is the absolute temperature,  $M$  the molecular weight and  $R$  the gas constant. Equation (1.51) becomes

$$\frac{R\theta\rho}{M} \ln \frac{P}{P_0} = \frac{2S}{a} + \frac{ds}{da} - \frac{q^2}{8\pi\epsilon_1 a^4} \quad (1.52)$$

If we assume that surface tension  $S$  is independent of the drop radius then we can set  $dS/da = 0$  in (1.52). Taking into account the dielectric constant  $\epsilon_2$  of the condensed liquid, (1.52) is modified as

$$\frac{R\theta\rho}{M} \ln \frac{P}{P_0} = \frac{2S}{a} - \frac{q^2}{8\pi a^4} \left( \frac{1}{\epsilon_1} - \frac{1}{\epsilon_2} \right) \quad (1.53)$$

The variation of the equilibrium super-saturation,  $p/p_0$  with drop radius  $a$  is shown in Fig. 1.30.  $a_1$  is the equilibrium radius of the drop and  $a_0$  is the value for which  $p = p_0$ . The values of  $a_0$  and  $a_1$  are given by the expressions

$$a_0^3 = \frac{q^2}{16\pi S} \left( \frac{1}{\epsilon_1} - \frac{1}{\epsilon_2} \right) \quad (1.54)$$

$$a_1^3 = \frac{q^2}{4\pi S} \left( \frac{1}{\epsilon_1} - \frac{1}{\epsilon_2} \right) \quad (1.55)$$

Each point in the diagram represents the condition of a drop of given radius in vapor at given pressure. The curve divides the space of the diagram into two parts.

Points above the curve represent the domain of drop growth (condensation) and those below correspond to evaporation. The curve itself is a stability curve. Consider a typical point *A* on the diagram. Condensation makes it move on the stability curve where further growth stops. The drop however, may be still invisible. On the other hand, a point like *B* does not hit the curve and moves from it indefinitely due to continuous growth. In a cloud chamber drops of class *B* do not exist initially but due to adiabatic expansion drops belonging to class *A* which are present pass over to class *B* if the super-saturation obtained is greater than the equilibrium value of radius  $a_1$ .

For water at 0 °C, for a drop carrying a single electronic charge,  $a_1 \cong 6 \times 10^{-10}$  m, for which  $(\frac{P}{P_0})_{a_1} = 4.2$ . Super saturation is produced by a rapid, adiabatic expansion of the mixture of gas and vapor. Most of the cloud chambers work by volume expansion. If  $\theta_1$  is the initial absolute temperature,  $\theta_2$  the final temperature,  $V_1$  the initial volume and  $V_2$  the final volume,  $\gamma = C_p/C_v$ , the ratio of specific heats at constant pressure and constant volume of the gas mixture, then:

$$\frac{\theta_1}{\theta_2} = \left( \frac{V_1}{V_2} \right)^{\gamma-1} \quad (1.56)$$

The change in temperature obviously depends on the value of  $\gamma$ . Because of a larger value of  $\gamma$  monatomic gases are preferably used. Most of the cloud chambers work on volume expansion by a mechanical device. But pressure defined chambers have also been used, specially in chambers containing metal plates. The pressure expansion is accomplished with only a thin rubber diaphragm separating the pressure vessels.

### 1.12.3 Choice of Pressure

Cloud chambers have been operated at pressures ranging from 1 atmosphere to 50 atmospheres. At low pressure, the vapor occupies a substantial fraction of the total amount of gas present, causing a change in the value of  $\gamma$  and results in an appreciable amount of ionization. Operation of the cloud chamber in the range of pressures 0.1 to 2.0 atm does not present any serious difficulties. At higher pressures, it is more difficult to remove old droplets and necessary waiting time between expansions increases with the increasing pressure. Curvature measurements in a magnetic field are rendered less accurate due to Coulomb multiple scattering of a charged particle in the high density gas.

### 1.12.4 Choice of Gas

Generally, noble gases are preferred because of lower expansion ratio required. Argon or a mixture of 50 % Argon and 50 % Helium are commonly used as they give clear tracks and rapidly growing droplets.

### ***1.12.5 Curvature Measurements***

A magnetic field is normally employed for momentum determination by curvature measurement. A large field is used so that spurious curvatures due to scattering and molecular motion are relatively less important. The maximum detectable momentum is that for which the uncertainty in the curvature is equal to the true curvature. With a field of 10 kG, momentum as large as 50 GeV/ $c$  has been measured over a track of 40 cm.

### ***1.12.6 Multiplate Chamber***

Since the stopping power is so low in a gas and the probability of interaction so small that in certain specific experiments it becomes necessary to place a set of metal plates in parallel planes leaving space in between so that the tracks can be recorded. Such multiplate chambers have proved to be invaluable in the investigations of nuclear reactions, and the short lived unstable particles produced in the reactions. The range of particles can be measured if the particle stops in one of the plates. In a multi-plate chamber  $\gamma$ -rays are materialized with much greater probability. Also the details of nuclear reactions can be studied.

### ***1.12.7 Counter Control***

It is a great advantage to use counter control expansions if rare events are to be studied. The expansion is effected only when a charged particle passes through associated counters in coincidence or anti-coincidence. Since expansion speeds are of the order of 10 milliseconds, counter controlled tracks are broadened by diffusion to widths of the order of a mm.

### ***1.12.8 Temperature Control***

In order to make accurate momentum measurements the gas in the chamber should be stable. This is accomplished by maintaining a temperature gradient of about 0.01 °C from top to bottom.

### ***1.12.9 Expansion Speed***

The speed of expansion of cloud chamber is an important consideration only for counter control type in which the width of the track may become too wide for accurate measurements. Tracks about 1 mm wide are obtained with expansion times of 14 milliseconds in air at N.T.P.

### 1.12.10 Recycling Time

An expansion cloud chamber normally takes at least one minute to prepare for each expansion. This time is used up for slow clearing expansions in order that the motion of the gas may subside and the vapor to diffuse back through the gas. Such repetition rates can not match the frequency of pulsed accelerators and in this regard they are inferior to bubble chambers which are capable of recycling every few seconds.

### 1.12.11 Discoveries

Expansion cloud chambers have played important role in the fundamental discoveries in Cosmic rays and Particle Physics. The penetrating nature of cosmic radiation was first established in 1932. The positron was discovered in 1933. The muon was confirmed and the  $K^+$  meson was discovered in 1944, and the two-pion decay mode in 1953. The so-called “V” events comprising kaons and hyperons were first identified in a cloud chamber as early as 1947 and the cascade hyperon in 1952.

## 1.13 Diffusion Cloud Chamber

### 1.13.1 Principle

A diffusion cloud chamber works on the principle of diffusion of condensable vapor from a warm region where it is not saturated to a cold region which is supersaturated and proper conditions are produced for the growth of droplets around ions similar to the expansion cloud chamber. The vapor density increases with temperature, while the gas density decreases with the increase in temperature. A given mixture of gas and vapor may thus have density that increases or decreases with the temperature depending on the composition. It is necessary to maintain density gradient in the chamber such that the density of the mixture is less at the top than at the bottom to avoid convection turbulence. Most of the diffusion chambers conveniently provide downward diffusion. The top is warm and it is here that vapor is introduced, and the bottom is cold. Figure 1.31 shows the essential details of a diffusion cloud chamber.

The body of the chamber containing the gas-vapor mixture is thermally connected to the base which is cooled to some low temperature  $T_0$ . A trough containing liquid which is vaporized by maintaining it at some temperature  $T_1$  higher than  $T_0$  is in contact with the glass top of the chamber. A temperature gradient is thus set up between top and bottom of the chamber. The gas at the top of the chamber is saturated with the vapor of the liquid contained in the trough. This vapor will diffuse towards the cooled base.

At the lower temperature the gas becomes supersaturated with the vapor. As the temperature decreases the value of super saturation increases. With a suitable gas-vapor ratio and the choice of  $T_1$  and  $T_0$ , the super saturation ( $S$ ) can exceed the

**Fig. 1.31** Diffusion cloud chamber

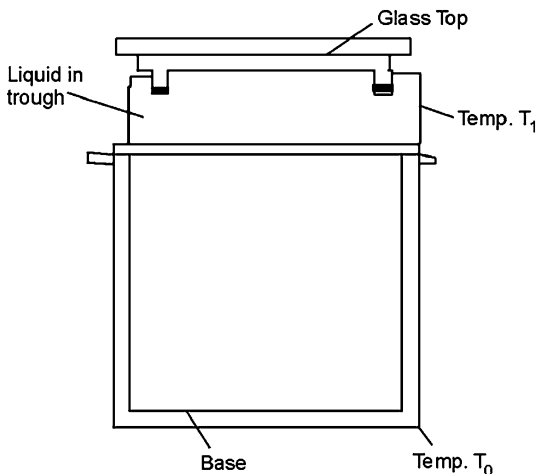
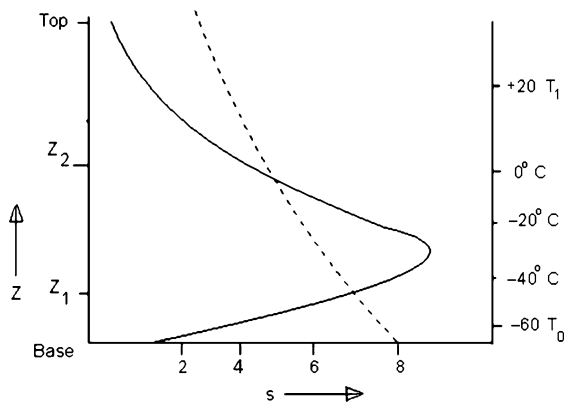


**Fig. 1.32** The *solid line* is a plot of  $S$  vs.  $Z$ ; the *dotted line* is the  $S$  vs.  $T$  curve



critical value necessary for condensation around ions. It can be shown (Thompson) that

$$\ln S = \frac{3M}{2RT\rho} \frac{(4\pi\sigma^4)^{\frac{1}{3}}}{(Kq^2)} \quad (1.57)$$

where  $M$  is the gram molecular weight,  $\rho$  the density,  $S$  the surface tension,  $K$  the dielectric constant of the liquid,  $T$  the absolute temperature,  $R$  the gas constant and  $q$  the charge carried by the ions. The saturation values resulting from certain temperature and vapor density distributions within the chamber are determined. For a given base temperature  $T$ , a typical curve for  $S$  versus  $Z$  (the chamber height) is shown in Fig. 1.32 by the solid line. The dotted curve ( $S$  vs  $T$ ) calculated from formula (1.57) for a typical liquid is also shown. The values of  $Z$  where the two curves intersect correspond to maximum height ( $Z_2$ ) and minimum height ( $Z_1$ ) in the cloud chamber at which the dropwise condensation upon ions is expected to occur. The region between  $Z_2$  and  $Z_1$  is the sensitive depth of the chamber.

### ***1.13.2 Choice of Liquid Vapor***

The operation of the diffusion chamber depends on large changes of vapor pressure with temperature. The choice of liquids is dictated by this property, over a convenient range of temperatures. It is desirable that the liquid has a low latent heat of vaporization so that the thermal equilibrium in the chamber is not disturbed due to the heat released from drop formation. Further, the liquid must have a low value for the critical vapor pressure necessary to sustain drop growth on ions. Methyl alcohol is a satisfactory liquid over the range of temperatures  $+30\text{ }^{\circ}\text{C}$  to  $-70\text{ }^{\circ}\text{C}$ . Ethyl alcohol is only slightly inferior for this purpose, while water is avoided as it freezes at a temperature within the range normally employed.

### ***1.13.3 Choice of Gas***

Chambers containing heavy gases like air or argon are useful only up to two or three atmospheres. According to Shut if air is used at 3 atm, with base at dry ice temperature, the top must be at a temperature around 293 K. If the temperature at the top is higher than this value, the sensitive region tends to become unstable and turbulent and it leads to background fog. The stability of gas is important from the point of view of curvature measurements.

Chambers containing light gas like hydrogen, deuterium and Helium are unsuitable at atmospheric pressure but become useful at pressures of 20 to 30 atm.

### ***1.13.4 Operating Temperatures***

With few exceptions, diffusion chambers have been operated with dry ice for the base temperature ( $-70\text{ }^{\circ}\text{C}$ ) and top temperature up to about  $30\text{ }^{\circ}\text{C}$ .

### ***1.13.5 Clearing Fields***

Apart from dust particles, there will be background due to neutral condensation nuclei and droplets formed on ions which have diffused into the sensitive region. The application of electric field between a grid of wires located just above the sensitive region and the top plate of the chamber enables the ions formed in the non-sensitive region to be collected by either electrode depending on the polarity. This method reduces the number of ions diffusing in the region and therefore considerably improves the track-to-background contrast. Dust particles and reevaporation nuclei are removed by continuous production of super-saturation until the nuclei are carried to the bottom of the chamber where they stick to the wall.

### ***1.13.6 Magnetic Field***

Momentum of a particle is determined by employing a magnetic field. A uniform field along the vertical axis may be produced either by a pair of Helmholtz coils placed around the chamber or by placing the chamber between the poles of an iron cored magnet.

### ***1.13.7 Photography***

Tracks may be photographed with a cine-camera under continuous illumination. Filters are necessary to avoid heating of the gas in the chamber. Alternatively, single shot photography may be employed using standard flash camera. A time delay of 0.1 to 0.2 sec is necessary between the ion formation and photography as the drops must be allowed to grow to a size which will scatter adequate light, but the delay must be kept to a minimum so that the falling of drops under gravity does not lead to serious distortion of tracks and there by destroy the accuracy of measurements.

### ***1.13.8 Advantages***

#### **1.13.8.1 Versatility**

Diffusion cloud chambers, when operated under suitable conditions provide information on the charge, momentum, velocity, life time, flux, direction of motion and the details of nuclear interactions. They have been operated at low atmospheric and high pressures in conjunction with high energy accelerators, in mines, on mountains and in balloons 100,000 ft above the earth.

#### **1.13.8.2 Use of Hydrogen**

Diffusion chambers using hydrogen at high pressures can be conveniently used to investigate elementary interactions with protons in Particle Physics. In contrast it is difficult to operate expansion cloud chamber with hydrogen filling at high pressure.

#### **1.13.8.3 Recycling Time**

In the diffusion chamber the re-cycling time for heavy gases is only 5–10 s, in contrast with the expansion chamber where it is 1–2 minutes. In pressurized hydrogen chambers, the contrast is still greater. This then means that comparatively short time is spent in taking photographs of desired events, there by saving expensive running time of the particle accelerator.



### **1.13.8.4 Counter Control**

Diffusion chambers may also be used with counter control. It is only necessary to trigger the camera to record the desired event.

### **1.13.8.5 Experiments with Accelerators**

As the sensitive region lies in the horizontal plane, diffusion chambers are ideally suited for investigations in Nuclear Physics and Particle Physics at the accelerators as the beams from the accelerators are in the horizontal direction.

## ***1.13.9 Limitations***

### **1.13.9.1 Cosmic Rays Studies**

The sensitive layer is not more than 3 inch thick and can not be made vertical for cosmic rays investigations.

### **1.13.9.2 Depletion of Vapor**

The passage of high flux of ionizing particles causes depletion of vapor, resulting in gaps in tracks. This is a serious problem in most diffusion chambers.

### **1.13.9.3 Ionization Limitations**

When the overall ionization within the chamber arising from various causes exceeds a certain level, the chamber will be rendered insensitive due to inadequate super saturation.

### **1.13.9.4 Foil Limitation**

When foils are used in a diffusion chamber, similar to multi-plate expansion cloud chamber, their design is limited in that they should not interfere with the temperature gradient. Thin strips of material of poor thermal conductivity fulfill this condition. Difficulties of turbulence are not a serious problem in diffusion chamber in contrast with the expansion chambers.

### ***1.13.10 Discoveries***

Some of the important experiments made with diffusion chambers are concerned with  $\pi^- p$  scattering, V-particle production in  $\pi^- p$  collisions, confirmation of Associated production of Strange particles, first direct evidence on multiple meson production in n-p collisions and Internal pair production of mesic  $\gamma$ -rays produced in slow  $\pi^-$  capture in hydrogen.

## **1.14 Bubble Chamber**

### ***1.14.1 Principle***

We owe the invention of bubble chamber to D.A. Glaser who conceived the idea that nucleation centers may be produced due to the passage of a charged particle in a superheated liquid so that a string of bubbles may be formed along the track. A superheated liquid is the one which is heated above the boiling point without actually boiling. The nucleation centre are formed due to the deposit of energy along the track of the ionizing particle. The superheated liquid is unstable and erupts into boiling shortly after formation of nucleation centers and the bubbles appear. The action of bubble chamber is the inverse of an expansion cloud chamber, with a gas bubble forming in a superheated liquid instead of a liquid drop forming in a superheated gas.

The liquid in a bubble chamber is superheated by a sudden expansion leading to a reduction of pressure. After the track is formed and photograph taken, the pressure is increased to the initial value by contracting the chamber. The bubbles collapse and the chamber is ready for another expansion. All this takes place in the matter of a few seconds such that the operation rate may advantageously match the frequency of particle beam from a pulsed accelerator in its duty cycle.

### ***1.14.2 Bubble Chamber Liquids***

A wide variety of pure liquids, liquid mixtures, and liquids containing dissolved gases have been used in bubble chamber. They range from hydrogen with a density of  $0.0586 \text{ gm/cm}^3$  and radiation length of 1100 cm to xenon with density  $2.3 \text{ gm/cm}^3$  and radiation length 3.7 cm.

#### **1.14.2.1 Hydrogen**

This is by far the most important liquid from the point of view of the elementary particle processes as the target contains pure protons. However, this advantage is offset by serious cryogenic problems as the operating temperature is around 28 K, and pressure 5–7 atm.

### 1.14.2.2 Deuterium

This is the lightest element containing neutron, and the liquid can be used in a chamber similar to hydrogen at operating temperature 32 K.

### 1.14.2.3 Helium

It is the lightest atom that has nuclear spin 0 and iso-spin 0. The operating temperature is 3–4 K and pressure  $\frac{1}{4}$  to 1 atm. Its merit is that it is non-flammable. However, the cryogenic problems are even more serious than those for hydrogen.

### 1.14.2.4 Propane (C<sub>3</sub>H<sub>8</sub>)

This is the most commonly used organic liquid operating at 58 K and at a pressure of 21 atm. The propane chambers are easier to build and operated compared to cryogenic chambers. However, the fire hazard is comparable with hydrogen chambers. The radiation length is down by a factor of 10. Although the amount of hydrogen in a propane chamber is greater by a factor of 1.38 than in hydrogen bubble chamber, it is difficult to isolate events in hydrogen from the carbon target.

### 1.14.2.5 Heavy Liquids

Liquids heavier than propane have been used for the study of  $\gamma$ -rays from  $\pi^0$  or  $\Sigma^0$ , through pair production. Suitable candidates are xenon (radiation length 3.7 cm), tungsten hexafluoride and freon, CF<sub>3</sub>Br (radiation length  $\sim 11$  cm). The last one mentioned is inexpensive, non-flammable and non-corrosive.

## 1.14.3 Control of Temperature

The temperature of a bubble chamber must be controlled to about 0.1 °C to ensure reproducible conditions.

## 1.14.4 Magnetic Field

Magnetic field is an important accessory of a bubble chamber for momentum measurement. For liquid hydrogen, multiple coulomb scattering is unimportant compared to the deflection in a magnetic field at 10 kG. Gauss or higher. In organic liquids, multiple scattering is more important and consequently at least 20 kG. Gauss

fields are employed for momentum measurements with an accuracy of 10 %. In heavy liquid chambers, multiple scattering is so severe that magnetic fields are rarely employed. Instead  $\rho\beta$  may be estimated from multiple scattering measurements as in emulsions. The mean second difference is given by

$$|\overline{D}| = \left( \frac{l^3}{X_0} \right) \times \frac{12.4}{\rho\beta} \quad (1.58)$$

However, the accuracy in momentum measurements is poorer by a factor of 10 compared to emulsions. If the curvature of a particle track in a magnetic field of  $B$  kG. Gauss is used to determine the particle momentum  $p$ , multiple scattering introduces an error  $\Delta p$  in the measurement of the momentum given by

$$\frac{\Delta P}{P} = \frac{4.1}{B\beta \sin \varphi \sqrt{X_0 l}} \quad (1.59)$$

where  $l$  is the length of track in space,  $\beta = v/c$ ,  $\varphi$  is the angle between the direction of the magnetic field and the momentum of the particle. In order to achieve an accuracy of 10 % in momentum measurement on a 10 cm track of a relativistic particle with a 15 kG. Gauss field, radiation length should not be less than 20 cm. For this reason magnetic fields are not used in heavy liquid bubble chambers.

### ***1.14.5 Track Distortion***

Liquid motion may displace the true track position following the bubble formation. In hydrogen bubble chamber a 1 GeV/c track can be distorted to the same extent as due to multiple Coulomb scattering.

### ***1.14.6 Number of Tracks per Picture***

In a single picture the higher density of bubble chamber liquids usually limits the number of tracks to 20 or 30 in order to obtain unambiguous events. This is in contrast with the cloud chamber in which 100 to 200 tracks can be used per picture. The bubble images are recorded by several stereoscopic cameras. Subsequent measurements of film are digitized, the tracks and vertices of event are reconstructed in three dimensions with the aid of a geometry program. Time resolution of the bubble chamber as determined from bubble size is measured in tens or hundreds of  $\mu$ S.

### ***1.14.7 Identification of Particles***

Measurement of curvature and residual range for particles which are arrested within the chamber permit the particles to be identified. This procedure is limited for protons of momentum less than 0.5 GeV/c. Ionization measurements are carried out by

bubble counting and are most valuable for protons of momentum 0.5 to 1 GeV/c.  $\delta$ -rays provide the best identification for protons between 1 to 3 GeV/c.

In heavy liquid bubble chambers curvature measurement is substituted by multiple Coulomb scattering measurements. They yield the value of  $p\beta$  (momentum times velocity). The combination of bubble density and curvature or bubble density and multiple scattering furnish the identification of particles.

### ***1.14.8 Advantages***

#### **1.14.8.1 Scanning**

Photographs of events can be easily scanned because of the large field of view and depth of focus. A large amount of data can be collected and analyzed in a short time. For the observation of a rare event sometimes it is necessary to examine more than hundred thousand photographs as in the discovery of  $\Omega^-$  and this has been possible in a bubble chamber of reasonably large volume. Further, bubble chambers are ideally suited to go with high energy accelerators.

#### **1.14.8.2 Mass Measurements and Correlation Studies**

The masses of particles can be estimated in most of the cases by the methods discussed in Sect. 1.11.4. Also the decays of neutral particles like  $K^0$ ,  $\Lambda$ ,  $\Sigma^0$  etc. can be correlated. This is rarely possible in emulsions.

#### **1.14.8.3 Fundamental Interactions with Protons**

The most important use of hydrogen bubble chamber is that it allows the studies of fundamental interactions with single protons, notwithstanding serious cryogenic problems.

#### **1.14.8.4 Special Target Nuclei**

Unambiguous interactions with neutrons can be studied in the deuterium bubble chamber, and specific interactions like the production of the hyper fragments  ${}^4\text{He}_\Lambda$  and  ${}^4\text{H}_\Lambda$  can be studied in helium bubble chamber with  $K^-$  beams.

#### **1.14.8.5 Background**

The short life time of nucleation centers (of the order of 1 millisecond) has the consequence of reducing the background of unwanted “old tracks”.

### **1.14.8.6 Gamma-Ray Detection**

$\gamma$ -rays can be detected through their materialization in heavy liquid chambers although their energy determination carries large uncertainty since radiation loss of electrons is both large and unpredictable. In xenon the average radiation energy loss amounts to 30 % per cm. Reliable momentum measurements require large  $X_0$  but conversion efficiency requires small  $X_0$ . The problem is solved with the use of a large propane bubble chambers with intermediate radiation length. Since the estimates of momentum obtained from curvature measurements and multiple Coulomb scattering are independent, it is possible to combine both types of measurements.

### **1.14.8.7 Re-cycling Time**

The re-cycling rates can be made to match the pulsed rate of accelerator beams.

## ***1.14.9 Limitations***

### **1.14.9.1 Tracks per Picture**

Number of tracks per picture can not exceed 20 or 30 for clarity.

### **1.14.9.2 Counter Control**

Since several milliseconds are required for the expansion, counter controlled expansions are not possible with the present techniques. For this reason bubble chambers have not been favored for cosmic ray studies where controlled expansion is often required. Also, bubble chambers can not be carried in balloons or rockets.

### **1.14.9.3 Spatial and Angular Resolution**

The spatial and angular resolutions of tracks are inferior to those in emulsions.

### **1.14.9.4 Use with Colliding Beam Accelerators**

As most of the modern accelerators are of colliding beam type, with a very low duty cycle of bubble chamber together with the geometry of the beams, they do not find a place for their utilization.

### ***1.14.10 Discoveries***

Numerous discoveries of fundamental nature in Particle Physics have been made with bubble chambers, particularly with hydrogen bubble chambers. These include the discoveries of the neutral cascade hyperon  $\Xi^0$  (1959), Anti-hyperon  $\bar{\Sigma}$  (1961),  $\bar{\Omega}^-$  (1962), the meson resonances  $\omega$ ,  $\rho$ ,  $\eta$  (1961),  $K^*$  meson (1963),  $Y^*$  (1964),  $\bar{\Omega}^+$  (1971), parity determination of  $K^-$  (1962) and  $K^0-\bar{K}^0$  regeneration (1961).

## **1.15 Spark Chamber**

### ***1.15.1 Principle***

To G. Charpak (1957) we owe the discovery of spark chamber in which electrical discharge occurs in narrow gaps of metal plates (maintained at large potential difference) following closely the trajectory of a charged particle.

### ***1.15.2 Mechanism of the Spark Discharge***

A free electron produced by ionization of the incident charge particle, in the presence of large field gradients, is accelerated until it strikes a gas molecule. With the repetition of this process number of free electrons increases exponentially. Simultaneously, space charge and diffusion result in a conical growth of the electron avalanche. This process continues until the space charge field at the head of the avalanche is of the order of external field. Positive-ion column left behind the head of avalanche produces photons resulting from the recombination. In turn more electrons are emitted from photo production. These electrons are rapidly accelerated into the space charge column as the space charge field and the external field act approximately in the same direction. This process results in further avalanches, and ultimately into self propagating streamers in the gap between the electrodes providing a highly conducting path through which a major discharge takes place. The initial electron avalanche lasts for  $10^{-7}$  to  $10^{-6}$  sec while the last part following the formation of streamers takes place in times of the order of  $10^{-10}$  to  $10^{-9}$  sec.

### ***1.15.3 Detection Efficiency***

#### **1.15.3.1 Detection Efficiency for a Single Particle**

For minimum ionizing particle at atmospheric pressure, about 8 ion pairs are formed per cm in Helium, 25 in Neon and 40 in Argon. According to Streamer theory, a

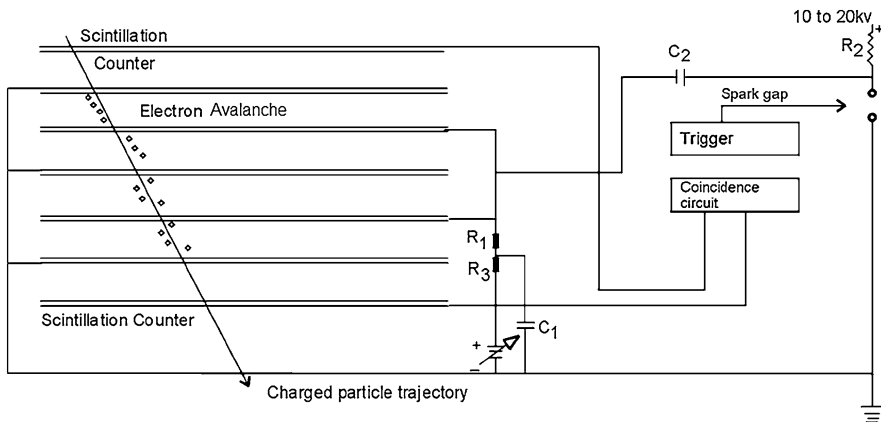


**Fig. 1.33** Block diagram of Spark chamber

single free electron leads to a discharge. The detection efficiency under favorable conditions may be close to unity. However, for a number of reasons the efficiency is lowered. Factors which contribute to lowering of efficiency are:

- i. Statistical fluctuations in ionization density specially at reduced pressure.
- ii. Gas impurities.
- iii. Delay in the application of high voltage pulse.
- iv. Poor rise time of high voltage pulse.
- v. Loss of energy from one gap by another gap not electrically decoupled.
- vi. Loss of energy by one or more extra sparks in the same gap.

### 1.15.3.2 Multiple Track Efficiency

In many experiments conducted with spark chambers specially in high energy physics it becomes necessary to detect correlated particles. When two or more sparks are in the same gap, efficiency may decrease as the first spark discharges the supply capacitor, Fig. 1.33, before the other spark(s) develops. In noble gases the breakdown times are reduced enormously with the increase in gap gradient, uniformity of gap width and use of large values for  $C_2$  capacitor (large discharge energies) generally improve the multi-track efficiency, at the expense of some definition of particle trajectory.

### 1.15.4 Time Resolution

Following the passage of a charged particle electrons and ions produced in the chamber gas recombine in times  $10^{-5}$  to  $10^{-4}$  sec. Electrons unrelated with the event



under observation must be removed as rapidly as possible. This is accomplished by applying low D.C. voltage across each gap. At 1 atm of noble gases, electric fields of the order of 100 V/cm will clear 1 cm gap in about  $10^{-6}$  sec. Alternatively, electronegative gases which capture free electrons can be introduced. Clearing times of the order of  $10^{-6}$  sec with the introduction of 1 %  $\text{SO}_2$  in neon can be achieved.

### ***1.15.5 Spatial Resolution***

Since ionization electrons of energy of several eV are produced, each electron diffuses in the time that elapses between the passage of the particle and the application of pulsed electric field. For typical delay times of  $3 \times 10^{-7}$  s the displacement is 0.8 mm, equal to the rms diffusion distance in neon. The apparent width of the spark is of the order of 1 mm.

### ***1.15.6 Effect of Magnetic Fields***

The use of large magnetic fields results in distinct changes in the performance of spark chamber:

- i. The electron diffusion rate across the magnetic lines is reduced. Thus, for example, the diffusion length in neon is reduced by a factor of about 2 in a field of 14 kG.
- ii. The clearing time for a given electric field is increased.
- iii. A transverse displacement velocity perpendicular to both electric and magnetic field causes a displacement away from the true path. In a Multi-gap chamber the displacement reverses its sign in alternate gaps as the polarity of electric field changes. The displacement problem can be eliminated by the use of electronegative gases.

### ***1.15.7 Recovery Time***

In the wake of spark discharge, electrons, ions and excited atoms in the gas must be avoided before the chamber is ready for another operation. This recovery time is typically 10 msec. Recovery time is reduced with the use of electronegative gases and clearing fields.

### ***1.15.8 Gas Composition***

A small percentage of contamination like oxygen adversely affects the performance of spark chamber. The electronegative impurities are favored for reasons discussed

earlier. Polyatomic gases like alcohol absorb ultraviolet arising from spark development. The inclusion of alcohol vapor to argon reduces spurious streamers, improves the quality of sparks and reduces the spark development time.

### ***1.15.9 Chamber Construction***

The chamber must be gas tight and electrically insulated.

### ***1.15.10 Tracks Inclined to the Electric Field***

For tracks inclined up to  $40^\circ$  to the electric field, sparks can follow the particle trajectory. With gaps up to 50 cm, and high voltage pulses 100 to 200 kV, sparks that following the particle trajectories to within 10 rad have been observed. Employing a magnetic field perpendicular to the electric field, particle momentum can be measured in a single gap.

### ***1.15.11 Applications***

#### **1.15.11.1 Counter Controlled**

The most important feature of spark chambers is that they can be counter-controlled with time resolutions less than  $10^{-6}$  s. The limit is set not so much by clearing time as by the necessary delays in the photomultiplier transit time, in cables, in the triggering circuit and high voltage pulsing circuits.

#### **1.15.11.2 Flexibility**

As a track detector, spark chamber is quite flexible in regard to size, shape and construction material, it has been used as a large-volume track detector of low mass and has been successfully used for cosmic rays investigations in air planes and balloons. On the other hand, multi-ton narrow-gap chambers have been constructed. To enhance the interaction rates, chambers with graphite plates have been employed for nucleon polarization measurements. With the use of heavy metal plates such as brass, iron, lead and tantalum, they have been used as electron and  $\gamma$ -ray detectors. Hydrogen target is furnished with the use of covered polyethylene.

### 1.15.11.3 Momentum Analysis

Momentum of high energy beam particles or secondaries can be analyzed with great precision. The momentum limit of the system is about  $2000 \text{ GeV}/c$ —a value which is an order of magnitude higher than that available in the operation of bubble chamber.

### 1.15.11.4 Analysis of Rare Events

When used in conjunction with scintillation and Cerenkov counters in the telescopic arrangement, spark chambers are amenable for locating rare events against heavy background. In the counter telescopic arrangement excellent spatial and time resolution of high energy particle interactions can be achieved. The chamber can be arranged to suite the experimental requirements.

### 1.15.11.5 Stereographic Photography

The intensity of light from the sparks is so great that stereographic photography is feasible even for a complex assembly of chambers.

## 1.15.12 Disadvantages

When narrow-gap chambers are used for analysis of low momentum secondaries or for analysis of decay products at rest or large angle decays in flight, the trajectories are inaccurately measured specially for particles at grazing angles to the electrodes.

## 1.15.13 Discoveries

Spark chamber has been used for the electron momentum measurement in muon decay (1969). Distinction between muon neutrino ( $\nu_\mu$ ) and electron neutrino ( $\nu_e$ ) was first established with the use of spark chambers by Schwartz, Lederman and Steinberger [2]. In 1964, Christenson et al. [3] observed CP violation ( $\sim 2 \times 10^{-3}$ ) employing spark chamber in conjunction with Cerenkov counter.

In 1970,  $e^+e^-$  ring (Mark I) was successfully constructed by SLAC-LBL collaboration. The heart of the detector was a spark chamber, a multi-purpose large solid angle magnetic detector which worked in conjunction with time-of-flight counters for particle velocity measurements, shower counters for photon detection and electron identification, and proportional counters embedded in iron absorber slabs for muon identification. Experiments conducted in 1974 with Mark I confirmed the

results of quark-parton model. Another important discovery was that of  $J/\psi$  resonance. Also, the decay mode  $\psi' \rightarrow \psi \pi^+ \pi^-$  was discovered by SLAC-LBL collaboration.

Further the discovery of Neutral Currents important for the electro-weak theory was made possible with the use of spark chamber. The neutrino detector at the Fermi Lab used 8 spark chambers and 16 liquid scintillator segments.

## 1.16 Calorimeters

### 1.16.1 Introduction

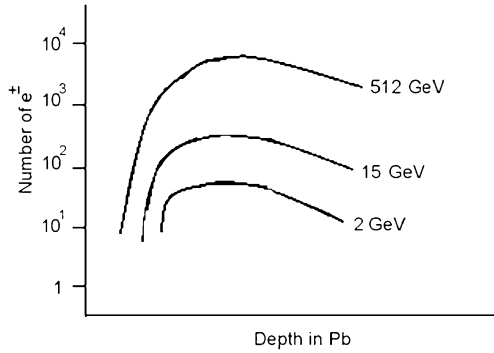
A device called calorimeter is a powerful and indispensable tool for the detection and energy measurement of very high-energy particles. In passing through the large mass of the detector, a particle is absorbed and produces secondaries which in turn produce tertiaries and so on. Thus, the particle energy is degraded through various processes and ultimately a substantial amount is lost to the calorimeter through ionization and excitation processes. The energy of the primary particle is determined by measuring the energy deposited in the ionization and excitation processes. Unlike other devices, like bubble chambers or ionization chambers, the particles are no longer available for further study. For this reason, calorimeters act as 'destructive' detectors. These devices permit the energy measurement of neutral hadrons (strongly interacting particles) as well as charged hadrons with great precision as the fractional energy resolution goes as  $E^{-1/2}$ , the precision at high energies (10–100 GeV) being comparable with what can be achieved from magnetic deflection. The position coordinates of the secondary particles may also be recorded under favourable conditions.

The characteristics of a calorimeter are determined by the nature of the dominant energy loss of the particles. For electrons and  $\gamma$ -rays, the energy loss is dominated by electromagnetic process—bremsstrahlung, pair production and Compton scattering. For hadrons, such as nucleons pions and kaons, nuclear interactions are primarily responsible for energy degradation. Thus Calorimeters fall into two categories—those which measure electron and  $\gamma$ -ray energies through electromagnetic processes and those which measure the energies of hadrons through nuclear interactions.

### 1.16.2 Electromagnetic Calorimeters

In the case of high energy electrons and photons a multiplicative process in the form of a cascade shower occurs, due to the combined effect of bremsstrahlung and pair production. A primary electron will radiate photons, which materialize to electron-positron pairs, which radiate and produce fresh pairs, the number of particles increasing exponentially with depth of the medium. The development and degradation of shower can be explained by a simplified model. Let the primary

**Fig. 1.34** The distribution of particles with depth in Pb for three primary energies



electron of energy  $E_0$  after traversing one radiation length  $X_0$ , radiate half the energy,  $E_0/2$  as one photon. Let after the next radiation length the photon convert to an electron–positron pair, each receiving half of the energy, i.e.  $E_0/4$ , and let the original electron further radiate a photon carrying half of energy  $E_0/4$ . Thus after two radiation length there will be a photon of energy  $E_0/4$ , two electrons and one positron, each of energy  $E_0/4$ . It follows that after  $t$  radiation lengths there will be  $N = 2^t$  particles, with photons, electrons and positrons approximately equal in number. Neglecting ionization loss and the dependence of radiation and pair production cross-section on energy, the energy per particle at depth  $t$  will then be  $\langle E \rangle = E_0/2^t$ . This process continues until  $\langle E \rangle = E_c$ , the critical energy when ionization loss at once becomes important and no further radiation is possible. The shower will thus reach a maximum and cease abruptly. The maximum will occur at the depth

$$t = t_{\max} = \frac{\ln(E_0/E_c)}{\ln 2} \quad (1.60)$$

The number of particles at the maximum will be

$$N_{\max} = \exp[t_{\max} \ln 2] = \frac{E_0}{E_c} \quad (1.61)$$

The total integral track length of charged particles (in radiation length) in the whole shower will be

$$L \simeq \frac{E_0}{E_c} \quad (1.62)$$

The shower particles continue to multiply until maximum number of particles is reached and the average particle energy is no longer high enough to continue the multiplication process. Beyond this point the shower decays as the particles lose energy by ionization and the photons by Compton scattering. The shower is characterized by an initial exponential rise, a broad maximum, and a gradual decline, see Fig. 1.34. Equations (1.60), (1.61) and (1.62) show

- i. a maximum at a depth increasing logarithmically with primary energy  $E_0$
- ii. the number of shower particles at the maximum being proportional to  $E_0$
- iii. a total track-length integral being proportional to  $E_0$ .

The radiation energy loss of electrons is characterized by the radiation length  $X_0$  defined by the relation.

$$E(t) = E_0 \exp\left(-\frac{t}{X_0}\right) \quad (1.63)$$

where  $E_0$  is the initial electron energy and  $E(t)$  the average energy after passing through a thickness  $t$  of material. Thus in traveling a thickness  $X_0$  the electron energy will be reduced by a factor of  $1/e$ . The corresponding length for pair production is found to be equal to  $9X_0/7$ .

In general,  $X_0$  is a function of electron energy and the nature of the absorber material. However for electron and photon energies above 1 GeV,  $X_0$  is practically independent of energy.

The dependence of  $X_0$  on the atomic number  $Z$  and mass number  $A$  is expressed by the formula

$$X_0 \text{ (g cm}^{-2}\text{)} \simeq 716 \frac{A}{Z^2} \ln(183Z^{-1/3}) \quad (1.64)$$

Since the logarithmic is a slow varying function,  $X_0$  decreases as  $Z^{-2}$  so that calorimeters employ high- $Z$  materials such as lead in order to minimize the overall size.

The multiple Coulomb scattering of electrons and positrons causes a radial spread of the shower from its axis (AAK, 1, 1). The processes of bremsstrahlung and pair production being predominantly peaked in the forward direction at high energies do not contribute significantly to the lateral (radial) spread. The radial spread is determined by  $R_M$  the Moliere unit which is defined by

$$R_M = (21 \text{ MeV}) \left( \frac{X_0}{E_c} \right) \quad (1.65)$$

where  $E_c$  is in MeV. About 90 % of the shower energy resides within  $R_M$  which is  $\sim 3X_0$  for Pb.

In order to use compact electromagnetic detectors materials of high  $Z$  and small  $X_0$  are used so that the shower may be contained within a small volume. Lead glass (55 % PbO, 45 % SiO<sub>2</sub>) is an important material for electromagnetic shower detectors. Cerenkov light from relativistic electrons is used to measure the shower energy.

The energy resolution is mainly determined by the fluctuations of the energy deposited in the active material. The resolution is determined by the fluctuations  $\sqrt{N}$  in the number  $N$  of particles at maximum, where  $N \propto E$ .

$$\frac{\Delta E}{E} = \frac{0.05}{\sqrt{E \text{ (GeV)}}} \quad (1.66)$$

These calorimeters are usually built of layers of absorbing material sandwiched by layers of detectors such as scintillator or ionization detector.

### 1.16.3 Hadron-Shower Calorimeters

A hadron shower is generated where an incident hadron suffers an inelastic collision producing secondary hadrons mostly pions ( $\pi^\pm, \pi^0$ ) which in turn lead through inelastic collisions tertiary generation of hadrons and so on.

Here the nuclear absorption length  $\lambda_0$  is the corresponding parameter in the electromagnetic calorimeters and is given by

$$\lambda_0 = \frac{1}{N\sigma} = \frac{A}{N_{av}\rho\sigma_i} \quad (1.67)$$

where  $N$  is the number of nuclei/unit volume,  $N_{av}$  is the Avogadro's number,  $\rho$  is the density,  $A$  is the mass number, and  $\sigma_i$  is the inelastic cross-section.  $\sigma_i$  and hence  $\lambda_0$  vary with energy near nucleon resonances but above 2 GeV is substantially constant. The scale of longitudinal development is determined by the nuclear absorption length  $\lambda_0$  ranging from 80 g cm<sup>-2</sup> for C through 130 g cm<sup>-2</sup> for Fe to 210 g cm<sup>-2</sup> for Pb. By comparison the scale is much larger than the radiation length for heavy elements,  $X_0 = 1.76$  cm for Fe and 0.56 for Pb.

For this reason hadron calorimeters have larger dimensions than for electromagnetic calorimeters. As an example an iron-scintillator sandwich has typically dimensions of order of 2 m and 0.5 m respectively.

In an electromagnetic cascade the bulk of energy is ultimately transformed into ionization which shows up as 'visible' (observed) energy. In the case of hadrons, however 30 % of the energy is unobserved as it goes into nuclear fragments, production of slow neutrons, and pion neutrinos which escape from the calorimeter. A large fraction of the energy can be recovered by introducing layers of U<sup>238</sup> into the calorimeter. Neutrons in the range of 1–10 MeV, typical for nuclear breakup cause fission in the U<sup>238</sup> nuclei and their energy is thus converted into charged particles whose ionization is measured.

The energy resolution of a hadron calorimeter is usually inferior than the electromagnetic calorimeter. This is due to much greater fluctuations in the development of the shower. The production of  $\pi^0$ 's in the early stage leads predominantly to electromagnetic cascade, of that of  $\pi^\pm$ 's predominantly to hadronic cascade, contributing substantially to the variation of energy that is deposited.

For hadron calorimeter

$$\frac{\Delta E}{E} \simeq \frac{0.5}{\sqrt{E}} \text{ (GeV)} \quad (1.68)$$

where  $E$  is the incident particle energy.

The lateral shower size is such that  $\sim 95$  % of the energy is deposited within a cylinder of radius  $\lambda_0$ , the mean free path.

Hadron calorimeters, similar to electromagnetic calorimeters, are constructed from a stack of alternate layers of absorbing material, such as iron or lead, and detectors such as scintillators or proportional counters.

In high-energy physics, typical experiments involve simultaneous detection, measurement and identification of several particles, both charged and neutral from

each interaction that occurs. It is usual to employ several types of detecting techniques, such as drift chambers for track position as well as ionization information, time of flight counters, muon detectors, electromagnetic and hadronic calorimeter etc. in a single assembly called a large hybrid detector, weighing 1000–10,000 tons.

### 1.17 Comparison of Various Experimental Techniques Used in High Energy Physics

Technique	Spatial Resolution	Time Resolution	Target	Interaction Rate	Triggable	Solid Angle
1. Scintillation Counter	$\geq 1$ cm	$\approx 10^{-9}$ s	Separate target	$10^6/\text{sec}$	Yes	$\ll 4\pi$
2. Cerenkov Counter	small	$\approx 10^{-9}$ s	Separate target		Yes	$\ll 4\pi$
3. Photographic Emulsion	1 $\mu\text{m}$	None	Ag, Br, H, C, N, O	MFP 30 cm	No	$4\pi$
4. Cloud Chamber (Expansion)	200–500 $\mu\text{m}$	100 ms	Mixture of gases	One interaction $\mu\text{m}$ per 100–1000 pictures	Yes	$4\pi$
5. Cloud Chamber (diffusion)	200–500 $\mu\text{m}$	Continuously sensitive	Mixture of gases	One interaction per 100–1000 pictures	Yes	$< 4\pi$
6. Spark Chamber	300 $\mu\text{m}$	$10^{-6}$ s	Separate target	20 triggers/sec	Yes	$\ll 4\pi$
7. Bubble Chamber	30 $\mu\text{m}$	$\approx 1$ ms	H <sub>2</sub> , D <sub>2</sub> C <sub>3</sub> H <sub>8</sub> , CF <sub>3</sub> Br, Xe	1 interaction per picture	No	$4\pi$

### 1.18 Questions

**1.1** Why ionization chambers with cylindrical geometry are to be preferred to plane electrode configuration?

**1.2** All the G.M. tubes have plateau with a small upward slope. Explain.



**1.3** G.M. tubes with halogen quenching have much longer life time than those with organic quenching vapors. Why?

**1.4** What happens if the ionization potential of quenching gas is greater than that of the main gas? Explain.

**1.5** What are  $4\pi$  proportional counters?

**1.6** What type of counter would you use to count  $\alpha$ 's against a background of  $\beta$ 's and  $\gamma$ -ray ?

- (a) pulsed ionization chamber
- (b) proportional counter
- (c) G.M. counter?

**1.7** Show that the capacitance of a cylindrical ion chamber is,  $C = \frac{2\pi\epsilon}{\ln(b/a)}$ .

**1.8** G.M. counters were taken to high altitudes to study cosmic ray studies. When they passed through Van Allen Radiation belts, they had stopped counting. Explain.

**1.9** In a surface barrier detector the energy resolution of particles or radiation is much better than in an ionized chamber. Explain.

**1.10** Why are the surface barrier detectors thus called?

**1.11** Why is germanium preferred to silicon for low energy  $\gamma$ -ray spectroscopy?

**1.12** When P-31 is irradiated by slow neutrons in a nuclear reactor, it is converted into radioactive phosphorus P-32 ( $T_{1/2} = 14.5D$ ). What should be the optimum time of irradiation so that a substantial amount of radioactive phosphorus is produced: (i) 1 week. (ii) 2 weeks. (iii) 10 weeks. (iv) 1 year. (v) 2 years?

**1.13** The  $n$ - $p$  scattering is known to be isotropic in the C.M. system at neutron energy of 3 MeV. What can you say about the energy distribution of recoil protons in Laboratory system?

**1.14** Why must photomultiplier tubes be cooled to low temperatures in experiments with scintillation counters?

**1.15** What is the difficulty in the use of inorganic phosphors with a large value of refractive index?

**1.16** Name three sources of background radiation experienced by an unshielded scintillator.

**1.17** If  $E_\gamma > 2mc^2$  (threshold for  $e^+e^-$  pair production) two new escape peaks are observed. Locate them.

**1.18** What is a counter telescope arrangement?

**1.19** What is time of flight method?

**1.20** What type of scintillator is used for the detection of a few MeV neutrons: (i) Organic? (ii) Inorganic?

**1.21** What is the dependence of velocity resolution  $\frac{\partial\theta}{\partial\beta}$  on the intensity of light emitted in the Cerenkov counter?

**1.22** The back-end of the cylindrical radiator of a Cerenkov counter is painted black. Explain.

**1.23** How do the chance coincidences compare for scintillation counters and Cerenkov counters?

**1.24** What is the function of gelatin in photographic emulsions?

**1.25** In what respect photographic emulsions are superior than other detectors in respect to (i) compactness? (ii) sensitivity? (iii) scanning? (iv) spatial and angular resolution? (v) a study of elementary interactions?

**1.26** Name three important discoveries that were made using photographic emulsion technique.

**1.27** It is difficult to make curvature measurements in magnetic field in photographic emulsions. Explain.

**1.28** Noble gases are generally used in expansion cloud chambers. Explain

**1.29** What is the function of a multi-plate expansion cloud chamber?

**1.30** In an expansion cloud chamber a small temperature gradient is maintained from top to bottom. Explain.

**1.31** Name three properties for the choice of liquid vapor in the operation of a diffusion cloud chamber.

**1.32** What kind of gases can be used at one or two atmospheres in a diffusion cloud chamber?

**1.33** How do the re-cycling times compare in expansion cloud chamber and diffusion chamber?

- 1.34** Name two important discoveries made with diffusion cloud chamber.
- 1.35** In what way is the study of neutral unstable particles through their decays more convenient in bubble chamber than in emulsions?
- 1.36** Name two liquids which are used for the detection of  $\gamma$ -rays in a bubble chamber.
- 1.37** Name three important discoveries made with bubble chamber.
- 1.38** Many new accelerators are of colliding beam type. Are the bubble chambers useful in this area as well?
- 1.39** Which of the following devices are operated counter-controlled?: (i) Expansion cloud chamber. (ii) Bubble chamber. (iii) Spark chamber. (iv) Emulsions?
- 1.40** Name two important discoveries made with Spark chamber.
- 1.41** Why are hadron calorimeters inferior than electromagnetic calorimeters?

## 1.19 Problems

- 1.1** An ionization chamber is connected to an electrometer of capacitance  $0.5 \mu\text{F}$  and voltage sensitivity of 4 divisions per volt. A beam of  $\alpha$ -particles causes a deflection of 0.8 divisions. Calculate the number of ion pairs required and the energy of the source of the  $\alpha$ -particles (1 ion pair requires energy of 35 eV,  $e = 1.6 \times 10^{-19}$  Coulomb)  
[Ans.  $6.25 \times 10^5$ , 21.9 MeV]
- 1.2** The dead time of a G.M. counter is 100  $\mu\text{s}$ . Find the true counting rate if the measured rate is 10,000 counts per min.  
[Ans. 10,169 per minute]
- 1.3** The dead time of a counter system is to be determined by taking measurements on two radioactive sources individually and collectively. If the pulse counts over a time interval  $t$  are, respectively,  $N_1$ ,  $N_2$  and  $N_{12}$ , what is the value of the dead time?
- 1.4** A certain G.M. counter has a dead time of 150  $\mu\text{s}$  after each discharge, during which a further particle entering is not detected. If its true counting rate is 32,432 cpm, what is the expected observed counting rate?  
[Ans. 30,000 cpm]
- 1.5** Suppose 200 mg of gold ( $^{197}\text{Au}$ ) foil are exposed to a thermal neutron flux of  $10^{12}$  neutrons  $\text{cm}^{-2}$  sec in a reactor. Calculate the activity and the number of atoms

of  $\text{Au}^{198}$  in the sample at equilibrium. (Thermal neutron activation cross section for  $\text{Au}^{198}$  is 98 barns and half-life for  $\text{Au}^{198}$  is 2.7 h.)

[Ans.  $3.08 \times 10^7$  dis/sec;  $2.24 \times 10^9$ ]

**1.6** A beam of neutrons of kinetic energy 0.29 eV, traverses normally a foil of  ${}_{92}\text{U}^{235}$  of thickness  $0.05 \text{ kg m}^{-2}$ . Calculate the attenuation of neutron beam by the foil ( $\sigma_s = 2 \times 10^{-30} \text{ m}^2$ ,  $\sigma_a = 7 \times 10^{-27} \text{ m}^2$ ,  $\sigma_f = 2 \times 10^{-26}$ ).

[Ans. 91.4 %]

**1.7** A  $\text{S}^{35}$  containing solution had a specific activity of 1 m. Curie per ml. A 20 ml sample of this solution mass was assayed.

- in a Geiger-Muller counter, when it registered 1500 cpm with a background count of 600 in 5 min; and
- in a liquid scintillation counter, where it registered 8200 cpm with a background count of 300 in 5 min.

Calculate the efficiency as applied to the measurement of radioactivity and discuss the factors responsible for the difference in efficiency of these two types of counter.

[Ans.  $3.8 \times 10^{-8}$ ;  $18.3 \times 10^{-8}$ ]

**1.8** A counter arrangement is set up for the identification of particles which originate from bombardment of a target with 5.3 GeV protons. The negatively charged particles are subjected to momentum analysis in a magnetic field, which permits only those having momentum  $p = 1.19 \text{ GeV}/c$  ( $\pm 2\%$ ) to pass through into a telescope system comprising two scintillation counters in coincidence with a separation of 12 m between the two detectors. Identify the particles, whose time of flight in the telescope arrangement was determined as  $t = 51 \pm 1 \text{ ns}$ . What would have been the time of flight of  $\pi^-$  mesons?

[Ans.  $p^-$ , 941 MeV; 40 ns]

**1.9** The peak resolution (full width at half maximum) of a germanium counter is 1.07 and 1.96 keV for  $\gamma$ -rays of energy 81 and 272 keV, respectively. Calculate the resolution at 662 keV.

[Ans. 3.06 keV]

**1.10** The 661 keV  $\gamma$ -rays from a radioactive source  ${}^{137}\text{Cs}$  are observed using a scintillation spectrometer and the pulse height spectrum shows a photo peak at 21.4 V. Determine the  $\gamma$ -ray energies from  ${}^{60}\text{Co}$  if the photo peaks occur at 37.9 V and 43.0 V.

[Ans. 1.17 MeV, 1.328 MeV]

**1.11** A sodium iodide crystal is used with a ten-stage photomultiplier to observe protons of energy 6 MeV. The phosphor gives one photon per 100 eV of energy loss. If the optical collection efficiency is 50 % and the conversion efficiency of the

photo-cathode is 5 %, calculate the average size and the standard deviation of the output voltage pulses when the mean gain per stage of the multiplier is 3 and the collector capacity is 10 pfs.

[Ans. 1.42 V]

**1.12** A 400-channel pulse-height analyzer has a dead time  $\tau = (17 + 0.5K) \mu\text{s}$  when it registers counts in channel  $K$ . How large may the pulse frequencies become if in channel 100 the dead time correction is not to exceed 10 %? Repeat the calculations for the channel 400.

[Ans. 1500/s; 460/s ]

**1.13** An anthracene crystal and a 12-stage photomultiplier tube are to be used as a scintillation spectrometer for  $\beta$ -rays. The phototube output circuit has a combined capacitance of 45 pf. If an 8-mV output pulse is desired whenever a 55-eV beta particle is incident on the crystal, calculate the electron multiplication required per stage. Assume perfect light collection and a photo-cathode efficiency of 5 %. (Assume 550 photons per beta particle.)

[Ans. 2.57]

**1.14** In an experiment using a Cerenkov counter, one measures the kinetic energy of a given particle species as  $E(\text{kin}) = 420 \text{ MeV}$  and observes that the Cerenkov angle in flint glass (refractive index  $\mu = 1.88$ ) is  $\theta = \arccos(0.55)$ . What particles are being detected (calculate their mass in  $m_e$  units).

[Ans.  $280.5m_e$ , Pion]

**1.15** Calculate the number of Cerenkov photons produced by a particle travelling at  $\beta = 0.95$  in water ( $\mu = 1.33$ ) in the response range (3500–5500 Å). Assuming 90 % light collection and 6 % photo-electrode conversion efficiency, what photomultiplier output signal would be produced?

**1.16** A proton of kinetic energy 40 keV enters a region where there is uniform electric field of  $4 \times 10^4 \text{ V/m}$ , acting perpendicularly to the velocity of the proton. What is the magnitude of a superimposed magnetic field that will result in no deflection of the proton?

[Ans. 144 gauss]

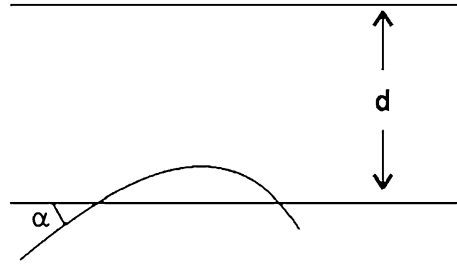
**1.17** A singly charged particle of speed  $0.3c$  gives a track of radius of curvature 100 cm under a uniform normal magnetic field of 1100 gauss. Calculate the rest mass of the particle, in terms of the electron mass  $m_e$  and identify it.

[Ans.  $M = 205m_e$ ; It is a muon]

**1.18** A fast (extremely relativistic) electron enters a capacitor at an angle  $\alpha$  as shown in Fig. 1.35.  $V$  is the voltage across the capacitor and  $d$  is the distance between plates. Give an equation for the path of the electron in the capacitor.

[Ans.  $y = x \tan \alpha - \frac{1}{2} V x^2 / mc^2 d \cos^2 \alpha$ ]

**Fig. 1.35** Electron moving across a capacitor



**1.19** A particle of known charge but unknown rest mass is accelerated from rest by an electric field  $E$  into a cloud chamber. After it has traveled a distance  $d$ , it leaves the electric field and enters a magnetic field  $B$  directed at right angles to  $E$ . From the radius of curvature of its path, show that the rest mass of the particle and the time it had taken to traverse the distance  $d$ , are given by  $qB^2r^2/2Ed$ ;  $t = Br/E$ .

**1.20** It is planned to use a mono-energetic  $k^-$  beam to perform reaction experiments with hydrogen target. Assuming that the beam transport system must have a minimum length of 30 m, calculate the minimum momentum of a kaon beam such that 5 % of the kaons accepted by the transport system arrive at the hydrogen target ( $\tau = 1.2 \times 10^{-8}$  sec,  $m_k = 494 \text{ MeV}/c^2$ ).

[Ans.  $1646 \text{ MeV}/c$ ]

## References

1. F.S. Goulding, Y. Stone, Science **170**, 280 (1970)
2. Schwartz, Lederman, Steinberger (1962)
3. Christenson et al. (1964)

Particle Physics

Kamal, A.

2014, XXII, 529 p. 275 illus., Hardcover

ISBN: 978-3-642-38660-2